

Characterizing spatiotemporal patterns of crop phenology across North America during 2000-2016 using satellite imagery and agricultural survey data

Yanjun Yang ^a, Wei Ren ^{a*}, Bo Tao ^{a*}, Lei Ji ^b, Liang Liang ^c, Alex C. Ruane ^d, Joshua B. Fisher ^e, Jiangui Liu ^f, Michael Sama ^g, Zhe Li ^h, and Qingjiu Tian ⁱ

^a Department of Plant and Soil Sciences, College of Agriculture, Food and Environment, University of Kentucky, KY 40546, USA;

^b ASRC Federal Data Solutions, contractor to USGS EROS Center, Sioux Falls, SD 57198, USA;

^c Department of Geography, College of Arts & Sciences, University of Kentucky, KY 40506, USA;

^d NASA Goddard Institute for Space Studies, New York, NY; 10025, USA;

^e Jet Propulsion Laboratory, California Institute of Technology, Pasadena, CA 91109, USA;

^f Ottawa Research and Development Centre, Agriculture and Agri-Food Canada, Ottawa, ON K1A0C6, Canada;

^g Department of Biosystems and Agricultural Engineering, College of Agriculture, Food and Environment, University of Kentucky, KY 40546, USA;

^h Center for Space Research, University of Texas at Austin, Austin, TX 78712, USA;

ⁱ International Institute for Earth System Science, Nanjing University, Nanjing 210023, China

* Correspondence: Wei Ren, wei.ren@uky.edu Tel: +1-859-257-1953; Bo Tao, bo.tao@uky.edu , Tel.: +1-859-218-6619

1 **Highlights:**

- 2 • Detected the major crop phenological stages using an improved EVI-curve-based approach
3 over North America during 2000-2016;
- 4 • Offered the first attempt to characterize the spatial and temporal patterns in crop phenology at
5 a continental scale;
- 6 • Crop planting and harvesting dates are highly correlated with the min/maximum temperatures.

7

8

9 **Abstract**

10 Crop phenology represents an integrative indicator of climate change and plays a vital role in
11 terrestrial carbon dynamics and sustainable agricultural development. However, spatiotemporal
12 variations of crop phenology remain unclear at large scales. This knowledge gap has hindered our
13 ability to realistically quantify the biogeochemical dynamics in agroecosystems, predict future
14 climate, and make informed decisions for climate change mitigation and adaptation. In this study,
15 we improved an EVI-curve-based approach and used it to detect spatiotemporal patterns in
16 cropping intensity and five major phenological stages over North America during 2000-2016 using
17 vegetation index in combination with agricultural survey data and other ancillary maps. Our
18 predicted crop phenological stages showed strong linear relationships with the survey-based
19 datasets, with R^2 , RMSEs, and MAEs in the ranges of 0.35 to 0.99, three to ten days, and two to
20 eight days, respectively. During the study period, the planting dates were advanced by 0.60
21 days/year ($p < 0.01$), and harvesting dates were delayed by 0.78 days/year ($p < 0.01$) over North
22 America. A minimum temperature increase by 1 °C caused a 4.26-day planting advance ($r = - 0.50$,
23 $p < 0.01$) or a 0.66-day harvest delay ($r = 0.10$, $p < 0.01$). While, a higher maximum temperature
24 resulted in a planting advance by 4.48 days/°C ($r = - 0.62$, $p < 0.01$) or a harvest advance by 2.22
25 days/°C ($r = - 0.40$, $p < 0.01$). Our analysis illustrated evident spatiotemporal variations in crop
26 phenology in response to climate change and management practices. The derived crop
27 phenological datasets and cropping intensity maps can be used in regional climate assessments and
28 in developing decision-making adaptation strategies.

29 **Keywords:** North America; crop phenology; cropping intensity; climate change; EVI-curve-based
30 approach; spatiotemporal trend analysis

31 **1. Introduction**

32 Vegetation phenology, defined as the development, differentiation, and initiation of plant organs
33 (Hodges, 1991), is an integrative indicator of climate change (Badeck et al., 2004). Changes in
34 vegetation phenology may have significant feedback to ecosystems and climate via the
35 biogeochemical (e.g., CO₂ releases or uptakes) and biophysical processes (e.g., albedo) (Jin et al.,
36 2013; Chen et al., 2015). Compared to natural vegetation phenology, crop phenology is more
37 complicated. It is regulated by not only natural factors (e.g., climate) but also intensive
38 management practices (e.g., cultivars and decisions on sowing dates) (Tao et al., 2012). Crop
39 phenology usually exhibits multiple cycles in a season as a result of diverse cropping systems and
40 multiple crop intensity (Li et al., 2014; Yan et al., 2014, 2019). Globally, agricultural fields occupy
41 approximately 37.2% of the global ice-free land surface, in which approximately 32% is used for
42 crop production (Ren et al., 2008). Accurate information of crop phenology over large areas is
43 crucial for advancing our understanding of agricultural ecosystem functioning and structure,
44 monitoring crop growth, realistically estimating carbon dynamics, and developing viable
45 management practices for climate adaptation and mitigation (Lobell et al., 2013; Diao, 2020;
46 Mercier et al., 2020).

47 In the context of climate change, shifted crop phenology, such as the advanced planting dates and
48 delayed harvesting dates, has been widely reported (Piao et al., 2006; Oteros et al., 2015; Sacks
49 and Kucharik, 2011). Generally, crop phenology information was mainly obtained from field
50 observations (Tao et al., 2006), remote sensing imagery (Xu et al., 2017), phenology modeling
51 (Liu et al., 2013), and survey data (Portmann et al., 2010). However, limited site-level observations
52 and district-based surveys (Sakamoto, et al., 2005) cannot fully capture highly variable patterns in
53 crop phenological stages over large areas (Piao et al., 2019; Zhang et al., 2020). Moreover,

54 phenology algorithms/models are usually fed by climate data such as temperature and soil moisture,
55 without or with relatively much fewer considerations about land management and practices (Tveito
56 et al., 2005; Wu et al., 2010). These limitations potentially bring large uncertainties to associated
57 climate impacts and carbon balance assessments at broad scales.

58 With rapid development in remote sensing over past decades, satellite imagery with worldwide
59 coverage and rapid re-visit times has made it possible to examine and monitor phenological
60 variations over large areas (Pan et al., 2015; White et al., 2014; Zeng et al., 2016; Zhang et al.,
61 2020). However, most crop phenology studies either constrained to a few specific crop types such
62 as wheat, corn, soybean, and rice (Xin et al., 2002; Lu et al., 2013) or targeted on limited crop
63 growing stages (e.g., the start or end of the season) (Liu et al., 2017). Moreover, crop phenological
64 stages (e.g., silking, denting, or mature dates) in multiple cropping systems with a rotation of one
65 or two crops per year have not been well addressed (Gumma et al., 2014). These knowledge gaps
66 have hindered our ability to understand the role of crop phenology in food production, surface
67 energy balance, and terrestrial biogeochemical cycles.

68 Over the recent decades, many methods have been developed to detect vegetation phenological
69 events using vegetation indices (VI) time series (Liu et al., 2016b; Zhu et al., 2012; White et al.,
70 2009). One of the essential processes of the satellite-based approach is to construct the VI time
71 series using various filtering algorithms such as the Fourier filter (Roerink et al., 2000), the
72 Savitzky-Golay filter (White et al., 2009), the asymmetric Gaussian function (Cong et al., 2012),
73 double logistic function (Zhang et al., 2003), and the Whittaker smoother (Atkinson et al., 2012).
74 Those functions can smooth out noise and fluctuations of the raw time series data, thus uncover
75 the temporal patterns of crop phenological stages (Diao, 2020). Based on the constructed time
76 series, crop phenological stages can be detected using various retrieval algorithms (e.g., inflection

77 or transition point, changing rate, and threshold-defined methods) (Zhang et al., 2003; Wang et al.,
78 2017).

79 The selection of the appropriate retrieval algorithms has substantial influences on estimated crop
80 phenological stages (Gao et al., 2017; Diao et al., 2020). Of the numerous methods, threshold-
81 based methods are often used because they generally keep dates within a specific reasonable range
82 based on the threshold conditions and achieve relatively higher accuracy. For example, You et al.
83 (2013) developed a threshold-based approach for identifying the start and end of the growing
84 season for 43 different agricultural zones in China using the AVHRR satellite data and observed
85 crop phenology at agro-meteorological stations. Although the threshold of each agricultural zone
86 can be determined to produce reasonable estimates of crop phenological timing, it is very
87 challenging to apply them directly over extended geographical regions, particularly for those
88 without enough detailed ground observations. Combined with ground observations, Huang et al.
89 (2019) demonstrated the importance of optimal thresholds for detecting crop phenological stages
90 at the site-level by evaluating the retrieval accuracy of crop start and end seasons using different
91 dynamic thresholds of VI time series. However, the site-level thresholds, to a large extent, cannot
92 capture the regional or global crop seasonal patterns, which calls for a more systematic approach
93 combining the advantages of the threshold-based method and characteristics of VI time series. This
94 systematic approach should be able to fit seasonal and annual fluctuations of multiple phenological
95 stages for major crop types at broader scales.

96 In this study, we used an EVI-curve-based approach for detecting spatiotemporal variations in the
97 cropping intensity and five major crop phenological stages (i.e., the dates of planting, jointing,
98 heading, maturity, and harvesting) of seven crop types over North America during 2000-2016. Our
99 overarching scientific objectives are to (1) improve an EVI-curve-based approach for detecting

100 changes in cropping intensity and dates of the five primary phenological stages at large scales; (2)
101 generate spatially explicit crop rotation and phenology datasets over North America during 2000-
102 2016; (3) characterize spatiotemporal variations of crop phenology and associated climatic driving
103 factors; and (4) identify uncertainties and future research needs.

104 **2. Materials and methods**

105 **2.1 Study area**

106 The spatial domain in this study covers North America (includes Canada, the United States, and
107 Mexico). Fertile soils, plentiful freshwater, and diverse climate all contribute to the agriculture
108 development of North America, making it one of the most important crop production areas in the
109 world. Its cultivated area occupies about 12.76% of the world's total acreage of cropland in 2016
110 (FAO, 2016) and covers more than 17% of the non-water, non-snow/ice areas of the entire
111 continent (Reed, 2013). The U.S. alone produces 46% of the world's corn and 33% of the world's
112 soybean, representing the largest corn and soybean producer (Taylor, 2015). North America spans
113 a range of latitudes and embraces diverse climates. Most of the continent has temperate climates
114 favorable to agriculture. In this study, North American croplands (including annual crops, woody
115 crops, and perennial crops and grasses) cover an area of 2,950,106 km².

116 **2.2 Datasets**

117 **2.2.1 MODIS data**

118 MODIS data have been widely used to monitor crop phenological changes (Thompson and Paull,
119 2017). In this study, crop phenological stages were retrieved for the continent of North America
120 using MODIS EVI (Enhanced Vegetation Index) time series from February 2000 to December
121 2016. EVI was calculated using the valid NIR (Near Infrared Reflectance), red and blue band

122 reflectance values from the land surface reflectance product MOD09A1 (version 6,
123 <ftp://ltdr.nascom.nasa.gov/allData>). MOD09A1 provides 500-m and 8-day composite surface
124 reflectance with seven bands in a Sinusoidal projection system, available from February 2000
125 through the present.

126 **2.2.2 Cropland distribution data**

127 The cropland distribution across North America was extracted from the 2005 and 2010 Land Cover
128 Database of North America at a spatial resolution of 250 m (<https://landcover.usgs.gov>). This
129 database was produced by the North American Land Change Monitoring System (NALCMS), a
130 trilateral effort among the Canada Centre for Remote Sensing (CCRS), the United States
131 Geological Survey (USGS), and three Mexican organizations, including the National Institute of
132 Statistics and Geography, National Commission for the Knowledge and Use of the Biodiversity
133 and the National Forestry Commission of Mexico. Cropland areas dominated by intensively
134 managed crops include areas used to produce annual crops, such as corn, soybeans, wheat,
135 vegetables, tobacco, and cotton; perennial grasses for grazing or forage; and woody crops like fruit
136 trees and grapevines. Because the continuous annual land cover dataset is not available for the
137 entire study area, we applied the 2005 land cover data for the period of 2000 - 2007 and the 2010
138 land cover data for the period of 2008 - 2016.

139 **2.2.3 Crop classification maps**

140 The crop classification maps were collected for validating the estimated crop phenology of
141 different crop types. For the United States, we used the Cropland Data Layers (CDL), a high-
142 resolution geo-referenced map made available by the U.S. Department of Agriculture (USDA).
143 The CDL combines remotely sensed data with the ground truth survey and provides multi-year
144 crop classification maps at a 30 m resolution for the conterminous United States

145 (<https://nassgeodata.gmu.edu/CropScape/>). The historical CDL goes back as early as 1997 for
146 North Dakota, and the national map was available from 2008 to the present
147 (https://www.nass.usda.gov/Research_and_Science/Cropland/metadata/meta.php). For Canada,
148 we used the Agriculture and Agri-Food Canada (AAFC) data, which was developed using a range
149 of high-resolution remotely sensed imagery (<https://open.canada.ca/data/en/dataset>). AAFC
150 dataset provides the annual crop inventory product at 30 m resolution (56 m for the period of 2009–
151 2010) across major agricultural regions in Canada during 2009-2017. The USDA CDL and AAFC
152 crop distribution maps were used for extracting sites across the U.S. and Canada agrarian regions.
153 For Mexico, there are no high-resolution crop classification time series maps available for the
154 validation purpose. Instead, the Mexico crop map was derived from the International Food Policy
155 Research Institute (IFPRI)'s Spatial Production Allocation Model (SPAM) Version 3.2, which
156 represents a global fractional distribution of major crop types at a 5-arc-minute resolution for the
157 period of 2004 - 2006 (You et al., 2014).

158 **2.2.4 Climate data**

159 Previous studies have indicated a strong relationship between the climate factors (e.g., average
160 maximum/minimum daily air temperature) and crop phenology (He et al., 2015; Rezaei et al., 2017;
161 Tao et al., 2006). In this study, we used daily spatially-interpolated air temperature from Daymet
162 (Thornton et al., 2017) to examine the relationships between climate changes and crop
163 phenological stages (planting dates and harvesting dates). The Daymet products provide estimates
164 of daily weather parameters at 1 km resolution for North America during 1980-2017. These
165 products have been widely used for biogeochemical modeling and climate change analysis at
166 regional to continental scales (Liu et al., 2016a).

167 All the spatial datasets we collected were reprojected to the Albers equal-area projection and
168 aggregated or downscaled to a 500 m resolution using the nearest neighbor algorithm in ArcGIS
169 10.3 to match the MODIS data.

170 **2.3 Inventories of crop phenology**

171 For the evaluation purpose, we collected ground data for the crop developmental stages from the
172 crop progress reports for the U.S., crop reports for Canada, and statistics data for Mexico
173 distributed by the USDA National Agricultural Statistics Service (NASS), Canada provincial
174 ministries (Alberta, Manitoba, Ontario, and Saskatchewan), and USDA Foreign Agricultural
175 Service (FAS), respectively. These data sets report typical crop growth dates categorized by crop
176 types at the state-level in the U.S., provincial level in Canada, and country-level in Mexico,
177 respectively. The USDA crop reports were updated weekly and averaged every five years and
178 covered the period of 2005 - 2016, with phenological stages for each crop type clearly defined
179 (https://www.nass.usda.gov/Publications/National_Crop_Progress/terms_definitions). These
180 reports provided the percentages of major crops reaching a specific crop development stage (e.g.,
181 maize planted or soybean harvested) over the entire area of a particular state. They had the
182 advantages of high reliability at the regional level. The dates of 80% progress of each recorded
183 stage for corn, soybean, spring wheat, and cotton were extracted from the crop progress and
184 condition graphs in USDA crop reports using the Web Plot Digitizer
185 (<https://automeris.io/WebPlotDigitizer>). For Canada, the crop reports only include the planting
186 dates and harvesting dates for four provinces, i.e., Alberta, Manitoba, Ontario, and Saskatchewan.
187 Provincial crop reports provide tables showing crop progress ranging from 20% to 100% at various
188 stages of barley, canola, soybean, spring wheat, and corn. All crop reports illustrated that the timing
189 of each crop phenological stage varied greatly depending on crop types and regions. For Mexico,

190 we used FAS statistics about crop planting and harvesting dates of corn and sorghum
191 (https://ipad.fas.usda.gov/rssiws/al/crop_calendar/ca.aspx) for evaluating those derived from this
192 study. Our collected data used for calibration and evaluation includes seven main crop types
193 covering the period of 2005 – 2016.

194 For the U.S. and Canada, we used five-year averaged crop phenology records from the
195 USDA/NASS to determine phenological thresholds and calibrate our improved approach.
196 Accordingly, the weekly records were extracted from crop reports for evaluating our estimated
197 crop phenological stages. For Mexico, the reported crop calendars in 2012 and 2017 were used for
198 threshold settings and results evaluation, respectively.

199 Besides, the cropping intensity information in the U.S. was extracted from the USDA CDL datasets
200 for validating the estimated crop rotation in this study. The satellite- and ground-based datasets
201 used in this study were summarized in Table 1.

202 **2.4 Methods**

203 **2.4.1 Deriving crop phenology descriptor**

204 The MODIS data process software (MODIS Reprojection Tool, MRT) available from
205 <http://edcdaac.usgs.gov/datatools.asp> was used to generate MOD09A1 products mosaics for North
206 America for each 8-day composite images, respectively (Ren et al., 2008). MODIS products were
207 re-projected from the sinusoidal projection to an Albers Equal-Area Conic projection, using the
208 nearest neighbor resampling method, and to a 500 m resolution using MRT (Huete et al., 2002).

209 The EVI was calculated from the reflectances of the RED, BLUE, and NIR bands as follows (Huete
210 et al., 1994).

$$211 \quad EVI = 2.5 \times \frac{\rho_{NIR} - \rho_{RED}}{\rho_{NIR} + 6.0 \times \rho_{RED} - 7.5 \times \rho_{BLUE} + 1.0} \quad (1)$$

212 Where ρ_{RED} , ρ_{NIR} , and ρ_{BLUE} are band 1 (0.620–0.670 μm), band 2 (0.841–0.876 μm), and band
213 3 (0.459–0.479 μm) reflectance from the MODIS products, respectively.

214 We first generated a cropland mask by aggregating the 250 m land cover dataset of North America
215 (see section 2.2.2) into 500 m and retained pixels with cropland percentages larger than 50%,
216 which could reduce the influences of mixed pixels on crop phenology detection. All EVI
217 processing and analyses were only conducted for cropland pixels for increasing computation
218 efficiency. The EVI time series were smoothed with HANTS_IDL (Harmonic Analysis of NDVI
219 Time Series). HANTS algorithm can smooth and reconstruct cloud-free remotely sensed
220 vegetation datasets, such as NDVI, EVI, and Leaf Area Index (LAI) time series, and reduce the
221 influence of clouds at the pixel level (Menenti et al., 1993; Zhang et al., 2015). Besides, it allows
222 greater flexibility in the frequency choices and time series length than the Fast Fourier Transform
223 (FFT) algorithm. HANTS is much more reliable than the straightforward FFT algorithm on
224 removing the obvious outliers of the time series datasets (Zhou et al., 2015).

225 The smoothing process needs two input files, i.e., the original EVI time series and a cropland mask
226 layer; only pixels with a value of 1 in the cropland mask layer were processed. Then the EVI time
227 series in croplands were smoothed, and other land cover types were masked out (Roerink et al.,
228 2000). Following these processes, the first and the second derivatives of the EVI curve were
229 defined as follows.

$$230 \quad f(x_i)' = \frac{f(x_i) - f(x_{i-1})}{8} \quad (2)$$

$$231 \quad f(x_i)'' = \frac{f(x_i)' - f(x_{i-1})'}{8} \quad (3)$$

232 Where, i is the sequence number of values in the time series (2, 3 ...46), the EVI curve has an

233 **Table 1** Summary of the Datasets Used in this Study.

Datasets	Spatial resolution	Timestep	Period	Data type	Data content	Purpose	Data source/description
MOD09A1	500m	8-day	2000-2016	Raster	Reflectance	Building EVI time series	LP DAAC
Land cover (NA)	250m	5-year	2005-2010	Raster	Cropland	Masking off non-cropland area	North American Land Change Monitoring System
Crop classification maps	30m/56m	Annual	2000-2016	Raster	Crop types	Providing individual map for evaluation of each crop type (U.S./Canada)	CDL of U.S./Agriculture Agri-Food Canada/Mexico
Meteorological data (NA)	1000m	Daily	2000-2016	Raster	Climate factors	Providing temporal climatic factors	Daymet
Global fractional distribution of major crop types (SPAM)	5-min	-	2004-2006	Raster	Crop types	Providing individual map for evaluation of each crop type (Mexico)	IFPRI
Crop reports (the U.S. and Canada)	State/Province	5-year average	2005-2016	Document	Crop phenology	Using for setting thresholds	USDA NASS
Crop reports (the U.S. and Canada)	State/Province	Weekly	2005-2016	Document	Crop phenology	Evaluating estimation accuracy	USDA NASS
Crop calendar maps (Mexico)	Country	Average	-	Document	Crop phenology	Setting thresholds (2012) and evaluating estimation accuracy (2017)	FAS
Global Agro-ecological Zones (GAEZ v3.0)	5-min	-	2012	Vector	Ecological zones	Analyzing temporal trend of crop phenology in each ecological zone	GAEZ Module

235 8-day time step, f and f' are smoothed and the first-order derivative of EVI time series,
236 respectively. Accordingly, the first and second derivatives have 45 and 44 time series values from
237 2th to 46th image (DOY, Day of Year from 9 to 365) and 3th to 46th image (DOY from 17 to 365),
238 respectively.

239 From equations (2) and (3), the lengths of the first and second derivatives were shortened compared
240 with the EVI time series. In this study, we did not make up the shortened periods because all
241 phenological stages of seven major crop types were not observed during the shortened periods
242 (DOY from 1 to 16) in North America (Appendix Table S1).

243 **2.4.2 Cropping intensity and crop phenology extraction algorithms**

244 In this study, the definitions of various crop phenological stages were from the USDA crop reports
245 (https://www.nass.usda.gov/Publications/National_Crop_Progress/terms_definitions, Table 2). It
246 has been widely accepted that EVI values could reflect the plant canopy development (Huete et
247 al., 1999; Jiang et al., 2008). The transition dates of VI time series curves could characterize the
248 seasonal dynamics of some crop growth stages, which have been used for identifying typical crop
249 phenological stages (Xin et al., 2002; Liu et al., 2017). Specifically, EVI can reduce sensitivity to
250 the soil, non-photosynthetically active vegetation, and atmospheric effects, but remains sensitive
251 to changes in canopy structure and density in cases where NDVI loses sensitivity (Zhang et al.,
252 2019).

253 In this study, we improved the EVI-curve-based approach through 1) using transition dates of the
254 EVI time series, first/second derivatives of the EVI time series to identify crop phenological stages;
255 2) setting flexible thresholds for five crop phenological stages according to the ground survey data;
256 3) expanding to detect five main crop phenological stages for seven crop types.

257 **Table 2** Phenology Definition of Different Crop Types.

Phenological stages	Crop types						
	Barley	Canola	Corn	Cotton	Soybean	Spring wheat	Sorghum
Planting	Planting	Planting	Planting	Planting	Planting	Planting	Planting
Jointing	-	-	-	Squaring	-	Jointing	-
Heading	Headed	-	Silking	Setting Bolls	Blooming	Headed	Headed
Mature	-	-	Mature	-	Dropping leave	Mature	Mature
Harvesting	Harvesting	Harvesting	Harvesting	Harvesting	Harvesting	Harvesting	Harvesting

258 *-Extracting cropland and cropping intensity*

259 Previous studies have verified that maximum NDVI occurs around the heading dates (Sakamoto
 260 et al., 2005; Xin et al., 2002). In this study, we took the EVI peaks as the heading date for each
 261 crop type (See the details in the section of Extracting five crop phenological stages). We set a
 262 maximum EVI threshold of 0.35 (Li et al., 2014; Liu et al., 2016a; Zhang et al., 2015) to exclude
 263 the non-croplands areas, i.e., the pixels with the maximum EVI values less than 0.35 were not
 264 included in the computation. Furthermore, we analyzed the ground data from crop reports and
 265 found that the intervals of two crop-heading dates in the double-cropping system were more than
 266 80 days across North America. This interval represents a useful parameter for determining a multi-
 267 cropping system (Sakamoto et al., 2006). Therefore, we set a threshold of 80-day for further
 268 identifying the double cropping system, i.e., if the interval between two EVI peaks is larger than
 269 80 days, the pixel will be identified as the double cropping system.

270 In addition, we also set a threshold for confining the time range of crop heading dates. The ground-
 271 based crop phenological information suggested that the heading dates of most crops occurred
 272 between the DOY (Day of Year) 150 and 260 in the U.S. (Appendix Table S1). Also, Sakamoto
 273 (2018) analyzed the EVI time series and detected the crop planting dates and harvesting dates as

274 60 days before the estimated heading dates and 30 days after the heading dates, respectively.
 275 Therefore, we set a more flexible time range (DOY, 73 ~ 297) as the threshold of heading dates
 276 for the entire North America. The peaks of the EVI curve falling outside this range were excluded.
 277 The criteria mentioned above can be described by the following conditions to identify cropping
 278 intensity:

$$279 \left\{ \begin{array}{l} f(x_i)' > 0 \\ f(x_{i+1})' < 0 \\ f(x_{i+1}) \geq 0.35 \\ 73 < T < 297 \\ \Delta T = T_i - T_j > 80, \text{ When } n \geq 2 \end{array} \right. \quad (4)$$

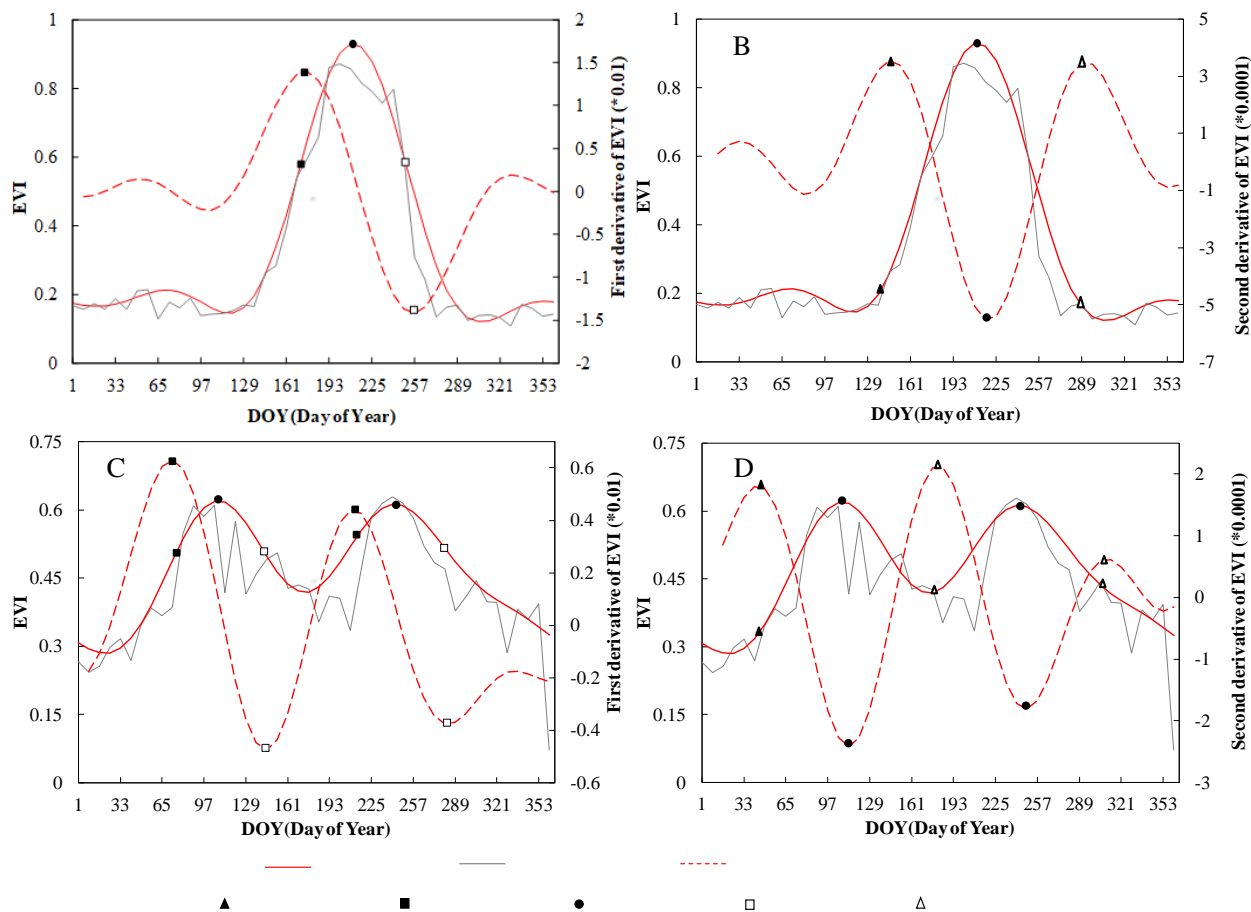
280 Where f' is the first-order derivative of EVI curve; f is smoothed EVI curve; i/j means the
 281 i th/ j th of EVI/EVI' values in the time series (1, 2, 3...46), T is the DOY of EVI peak, ΔT is the
 282 time interval of two peaks of the EVI curve. We, therefore, obtained cropping intensity n (Single-
 283 cropping system: $n = 1$ and double-cropping system: $n = 2$).

284 ***-Extracting five crop phenological stages***

285 *Heading dates*

286 The heading dates are reached when transforming from the vegetative stage to the reproductive
 287 stage, after which leaves begin to turn yellow and wither (Sakamoto et al., 2005). In this study, we
 288 identified the heading date (T_{heading1} for the single-cropping system and T_{heading1} , and T_{heading2} for
 289 the double-cropping system) as the date that the maximum MODIS EVI occurs in the time profiles
 290 (Xin et al., 2002; Xu et al., 2017; Yan et al., 2019). Based on the summarized ground data from
 291 crop reports (see section 2.3), we found that the crop growing season is typically less than 220
 292 days for major crop types (Appendix Table. S2). We thereby confined the crop growing season
 293 within the range of 110 days before and after the estimated heading date (Fig. 1; Appendix Fig.

294 S1; Table 3). The identification of the temporal thresholds for constraining predicted values can
 295 reduce the interferences caused by data noise.



296
 297 **Fig. 1.** Crop phenological stages extracted using the first and second derivatives of the EVI curve
 298 for the single-cropping system (A, B) and double cropping system (C, D).

299 *Planting dates*

300 In general, agricultural lands are plowed or cultivated before crop planting. At the planting dates,
 301 photosynthetic activity does not start, and crop leaves begin to grow after the planting dates. The
 302 EVI curve shows lower values during this period and then starts increasing after crop planting. It
 303 is reasonable to assume that the planting date is located at the lowest point of the EVI profile during
 304 the early growth stage. This lowest point corresponds to the peak of the second-order derivative of

305 the EVI curve (before the heading date), after which the EVI value begins to increase (Figs. 1B
306 and 1D). We then identified the crop planting dates by detecting when the second-order derivative
307 of the EVI curve reaches the first peak before the heading dates. Based on the ground data, the
308 planting dates were constrained to occur within the time range of 40 - 110 days before the estimated
309 heading dates (Table 3).

310 *Jointing dates*

311 The jointing dates occur after the planting dates and before the heading dates. At this stage, the
312 crop canopy expands rapidly to meet the active photosynthetic activity. Accordingly, EVI value
313 increases with a higher rate than other stages (Figs. 1A and 1C). In this study, we identified the
314 jointing date by detecting the peak of the first-order derivative of the EVI curve (before the heading
315 date), i.e., the fastest growing point of EVI values. To reduce the impact of outliers, we set a
316 threshold of 20 - 90 days before the heading dates by referring to the crop reports.

317 *Maturity dates*

318 The maturity dates take place during the period plant leaf begins to lose activity or change color
319 after the heading dates and before the harvesting dates. During this period, photosynthetic activity
320 and green leaf area decrease rapidly. The trough of the first-order derivative of the EVI curve (after
321 the heading date) represents the fastest declining point of EVI values. We then defined the point
322 in the EVI time series curve with a maximum reduction rate as the crop maturity dates (Figs. 1A
323 and 1C). Similar to other phenological stages, we also set an appropriate threshold with a range of
324 20 to 90 days after the heading dates for the maturity dates (Table 3).

325 *Harvesting dates*

326 In the harvesting season, leaves of crop plants continue to wither and die after the maturity stage.
327 Crop canopies are generally harvested in this stage. Correspondingly, EVI values continue to
328 decrease and go to the lowest point when the crop harvested from fields. The peak of the second-
329 order derivative of the EVI curve after the heading date corresponds to the lowest value of EVI
330 during the crop growth period (Figs. 1B and 1D). Here we used this key point to detect the
331 harvesting date. Similarly, based on the ground data, the harvesting dates were constrained to occur
332 within the time range of 30 - 110 days after the estimated heading dates.

333 All thresholds we used for identified five phenological stages (Table 3) were based on the ground
334 information recorded in crop reports (Appendix Table. S2). These thresholds represent the relative
335 time ranges, which depend on the dynamic pattern of the EVI curves.

336 Wheat-soybean is the most popular double cropping system in the study area (Marra and Carlson,
337 1986; Kelley et al., 2005; Borchers et al., 2014). Winter varieties were usually planted each fall
338 directly following soybean harvest in early October (Heggenstaller et al., 2008). USDA report
339 (Marra and Carlson, 1986) suggested that the winter wheat is generally harvested in the morning
340 and soybeans planted in the afternoon of the same day in the same field, especially when
341 conservation tillage is applied. In some cases, the growing season for the second cropping system
342 could be shortened because of the overlap in harvesting the first crop and planting the second
343 (Marra and Carlson, 1986). Therefore, in this study, we detected the harvesting date of the first
344 season as the planting date of the second season.

345 Fig.2 shows a study flowchart summarizing the systematic processes of identifying crop
346 phenological stages.

347

348 **Table 3** Transition Dates and Thresholds from Time Series Curves for Identifying Phenological
 349 Stages.

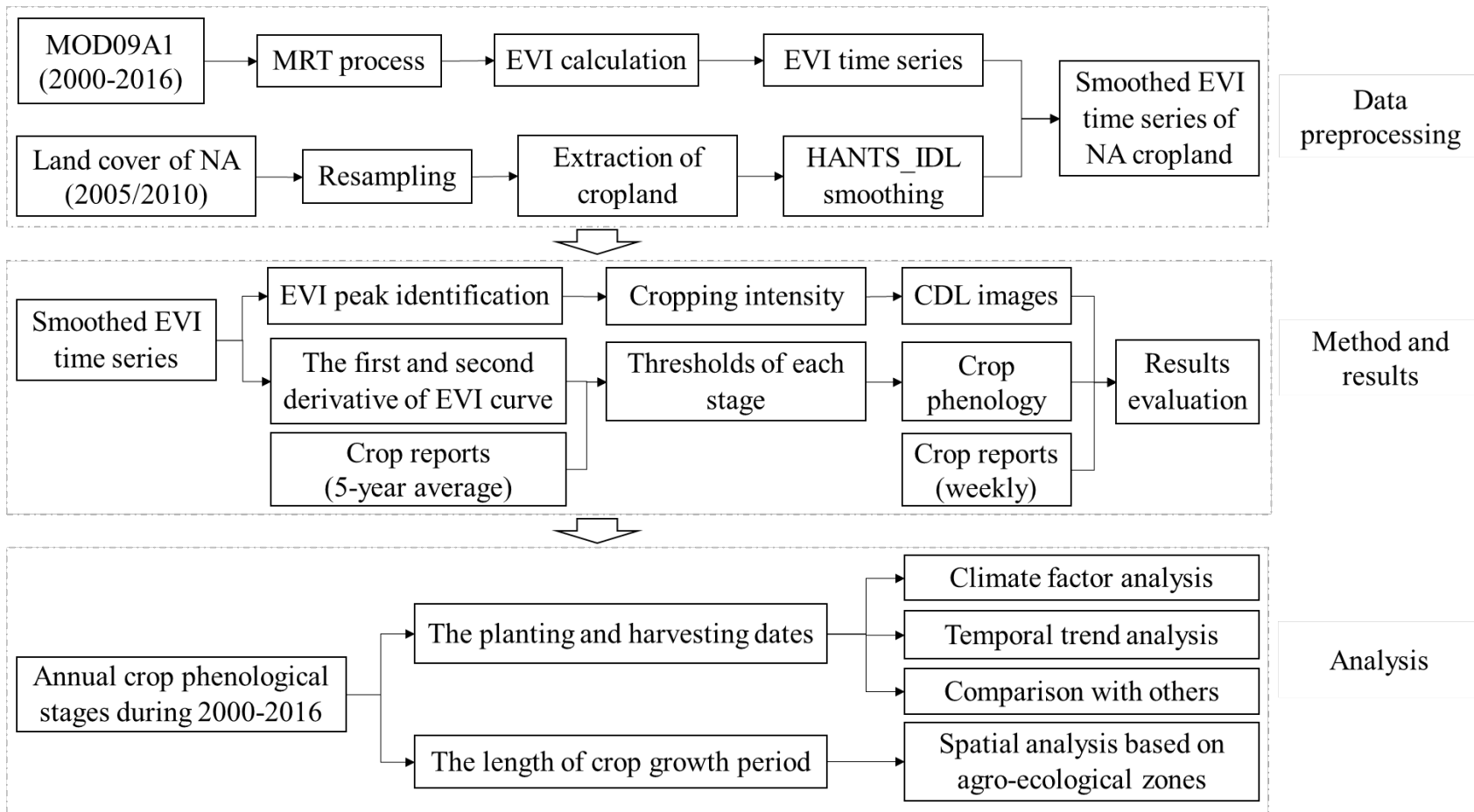
Phenological stages	Descriptions	Range with thresholds (Day of Year, DOY)
Heading: T_{heading1}	The first peak of EVI time series	
Planting: $T_{\text{planting1}}$	The peak of the 2nd derivative	$[T_{\text{heading1}} - 110, T_{\text{heading1}} - 40]$
Jointing: $T_{\text{jointing1}}$	The peak of the 1st derivative	$[T_{\text{heading1}} - 90, T_{\text{heading1}} - 20]$
Mature: $T_{\text{maturity1}}$	The trough of the 1st derivative	$[T_{\text{heading1}} + 20, T_{\text{heading1}} + 90]$
Harvesting: $T_{\text{harvesting1}}$	The peak of the 2nd derivative	$[T_{\text{heading1}} + 30, T_{\text{heading1}} + 110]$
Heading: T_{heading2}	The second peak of EVI time series	
Planting: $T_{\text{planting2}}$	The peak of the 2nd derivative	$[T_{\text{heading2}} - 110, T_{\text{heading2}} - 40]$
Jointing: $T_{\text{jointing2}}$	The peak of the 1st derivative	$[T_{\text{heading2}} - 90, T_{\text{heading2}} - 20]$
Mature: $T_{\text{maturity2}}$	The trough of the 1st derivative	$[T_{\text{heading2}} + 20, T_{\text{heading2}} + 90]$
Harvesting: $T_{\text{harvesting2}}$	The peak of 2nd derivative	$[T_{\text{heading2}} + 30, T_{\text{heading2}} + 110]$

350 2.5 Accuracy evaluation

351 2.5.1 Evaluation of the satellite-based cropping intensity

352 For evaluating the cropping intensity results, we randomly chose a total of 1006 sites, including
 353 the single-cropping system and the double-cropping system distributed across twelve regions in
 354 the United States based on the 2016 CDL data (Appendix Table S2). Each site consists of a polygon
 355 delineated on CDL maps via manual interpretation, ensuring that the verification datasets are
 356 widely distributed geographically. The size of the evaluation sites ranged from 1 pixel ($\sim 0.25 \text{ km}^2$)
 357 to 79 pixels ($\sim 19.75 \text{ km}^2$), and these sites covered 6,000 MODIS pixels.

358 The confusion matrix was applied to evaluate the estimated cropping intensity. It includes the
 359 overall accuracy (OA), Kappa coefficient (Kappa), producer's accuracy (PA), and user's accuracy



360

361 **Fig. 2.** Study flow chart.

362

363

364 (UA) (Fitzgerald et al., 1994; Næsset, E., 1996). The overall accuracy represents the percentage
 365 of estimated samples that are correctly identified (Hubert-Moy et al., 2001). The Kappa coefficient
 366 measures the agreement between observations and prediction results. Kappa coefficient value of 1
 367 represents a perfect agreement, while a value of 0 means no agreement. The producer's accuracy
 368 is a measure of the omission error, defined as the number of correctly classified pixels relative to
 369 the total number of pixels used in the assessment for a specific class. The user's accuracy is a
 370 measure of the commission error associated with a class, which is derived from the number of
 371 pixels correctly allocated to a class relative to the total number of pixels predicted to belong to that
 372 class (Foody, et al., 2006). Overall accuracy and the Kappa coefficient were computed as follows
 373 (Congalton, 1991):

$$\text{Overall Accuracy} = \frac{\text{Total number of correct estimaitons}}{\text{Total number of dataset}} \quad (5)$$

$$\text{Kappa} = \frac{N \sum_{i=1}^r x_{ii} - \sum_{i=1}^r (x_{i+} \times x_{+i})}{N^2 - \sum_{i=1}^r (x_{i+} \times x_{+i})} \quad (6)$$

374 Where r is the number of rows in the matrix, x_{ii} is the number of observations in row i and
 375 column i , x_{i+} and x_{+i} are the marginal totals of row i and column i , respectively, and N is the total
 376 number of observations.

377 **2.5.2 Evaluation of the satellite-based crop phenology**

378 We evaluated our estimated crop phenology results against ground information recorded in crop
 379 progress reports from USDA, NASS, Canada provinces, and FAO (Table 4). Crop classification
 380 maps used included CDL for the U.S., AAFC for Canada, and crop map derived from SPAM for
 381 Mexico. We summarized crop phenology of six main crop types (corn, soybean, spring wheat,
 382 barley, sorghum, and cotton) for the U.S. from USDA NASS crop progress reports, five major

383 crop types (barley, canola, soybean, spring wheat, and corn) for Canada from the crop reports of
 384 five provinces, and two crop types (corn and sorghum) for Mexico from the FAO reports (Table
 385 4). These seven crop types comprise more than 65% of the total crop area in North America (USDA
 386 NASS Census of Agriculture in 2017). For each crop type, we selected major producing states or
 387 provinces to evaluate estimated phenological stages (Table 4). In these states or provinces, we
 388 chose pixels that the targeted crop types accounted for more than 80% to compare against satellite-
 389 derived crop phenology. Limited by the data availability, we separately evaluated corn and
 390 soybean by randomly selecting 75 sites to assess the accuracy of satellite-based crop phenology in
 391 Mexico from 2004 to 2016. Pixels in the center of larger patches were selected to reduce the
 392 influence of mixed pixels during this process.

393 We used the coefficient of determination (R^2), root mean square error ($RMSE$), and mean absolute
 394 error (MAE) to evaluate the estimated crop phenological stages. In general, a higher R^2 , a lower
 395 $RMSE$, and a lower MAE mean higher accuracies of the estimation:

$$396 \quad R^2 = \frac{\sum_{i=1}^n (x_i - \bar{x})(y_i - \bar{y})^2}{\sum_{i=1}^n (x_i - \bar{x})^2 \sum_{i=1}^n (y_i - \bar{y})^2} \quad (7)$$

$$397 \quad RMSE = \sqrt{\frac{1}{n} \sum_{i=1}^n (y_i - x_i)^2} \quad (8)$$

$$398 \quad MAE = \frac{1}{n} \sum_{i=1}^n |y_i - x_i| \quad (9)$$

399 where n represents the number of comparisons; y_i and x_i are estimated phenological dates in this
 400 study and those derived from ground information, respectively.

401 **Table 4** Data Used for Estimated Phenological Stages Evaluation.

ID	Crop types	Years	Phenological stages	Countries	States/Provinces
1	Corn	2004-2016	Planting Heading Mature Harvesting	The U.S. Canada Mexico	Colorado; Ohio; Illinois; Indiana; Iowa; Kansas; Kentucky; Michigan; Minnesota; Missouri; Nebraska; North Dakota; South Dakota; Ontario Arkansas; Illinois; Indiana;
2	Soybean	2005-2016	Planting Heading Mature Harvesting	The U.S. Canada	Iowa; Kansas; Kentucky; Louisiana; Michigan; Minnesota; Mississippi; Ontario; Manitoba
3	Cotton	2006-2016	Planting Jointing Heading Harvesting	The U.S.	Alabama; Arizona; Arkansas; California; Georgia
4	Spring wheat	2005-2016	Planting Jointing Heading Mature Harvesting	The U.S. Canada	Idaho; Minnesota; Montana; North Dakota; South Dakota; Alberta; Saskatchewan; Manitoba
5	Barley	2009-2016	Planting Heading Harvesting	The U.S. Canada	Colorado; Montana; Oregon; Utah; Washington; Wyoming; Alberta; Saskatchewan; Manitoba
6	Canola	2009-2016	Planting Harvesting	Canada	Alberta; Manitoba; Saskatchewan; Ontario
7	Sorghum	2004-2006	Planting Heading Mature Harvesting	The U.S. Mexico	Colorado; Kansas; Oklahoma; South Dakota; Texas

402 **2.6 Mann–Kendall test and Sen’s slope estimator**

403 In this study, we used the Mann–Kendall test (Gilbert, 1987; Chmielewski et al., 2004; Li et al.,
404 2014) and the Sen’s slope estimator (Sen, 1968) to identify statistically significant monotonic
405 trends in estimated planting dates, harvesting dates, and length of the crop growing season. We
406 analyzed the temporal trends of crop planting and harvesting dates (the single cropping system and
407 the first season of the double cropping system) using the Mann-Kendall test and the Sen’s slope.
408 Further, we also tested the interannual variation of cropping systems in North America during the

409 study period. The statistical analysis was implemented using the R computing environment
 410 (Development Core Team, 2011).

411 We followed Sen (1968) to calculate the slope of the time series as:

$$412 \quad Q_{j,k} = \frac{x_j - x_k}{j - k} \quad (10)$$

413 Where, $k < j$, $k = 1, 2, \dots, n-1$, and $j = k + 1, k + 2, \dots, n$; x_j and x_k are the crop phenological
 414 stage for year j and k , respectively; n is the length of the time series.

415 Therefore, a total of $n(n - 1)/2$ elements of $Q_{j,k}$ and their median is the slope, or trend, of the
 416 temporal phenological stages series.

417 The significance of the slope was tested using the Mann–Kendall statistic (Gilbert, 1987), in which
 418 we first calculated the parameter S as:

$$419 \quad S = \sum_{k=1}^{n-1} \sum_{j=k+1}^n \text{sign}(x_j - x_k) \quad (11)$$

420 Where $\text{sign}(x_j - x_k)$ is -1, 0, or +1 if $(x_j - x_k)$ is < 0 , $= 0$, or > 0 , respectively. Then we calculated
 421 parameter V as:

$$422 \quad V = \frac{1}{18} [n(n - 1)(2n - 5) - \sum_{p=1}^g t_p(t_p - 1)(2t_p + 5)] \quad (12)$$

423 Where g is the number of tied groups. A tied group is a set of sample data that have the same value
 424 and t_p is the number of years in the p_{th} tied group. If there are no tied groups, this summation
 425 process can be ignored (Kisi and Ay, 2014). At last, the test statistic Z was calculated as:

$$426 \quad Z = \begin{cases} \frac{S-1}{\sqrt{V}}, & \text{if } S > 0 \\ 0, & \text{if } S = 0 \\ \frac{S+1}{\sqrt{V}}, & \text{if } S < 0 \end{cases} \quad (13)$$

427 Positive values of Z indicate increasing trends, while negative Z values show decreasing trends.
428 Testing trends was performed at the specific α significance level. If $Z > Z_{0.90} = 1.65$, $Z > Z_{0.95} =$
429 1.96 , or $Z > Z_{0.99} = 2.58$, the slope estimated by $Q_{j,k}$ is significant at 90%, 95%, and 99%
430 confidence level, respectively.

431 **2.7 Climate datasets**

432 To examine climate change impacts, we correlated our estimated crop phenology to daily air
433 temperatures over North America during 2000-2016. Average daily minimum/maximum
434 temperatures during crop planting season (April to June) and harvesting season (August to October)
435 were calculated based on the Daymet climate datasets (Thornton et al., 2017).

436 **3. Results**

437 **3.1 Evaluation of the satellite-based cropping intensity**

438 Based on the CDL datasets, we mapped the spatial distribution of the single- and double- cropping
439 systems using the feature extraction tool in ArcGIS 10.3. Accuracies of the estimated cropping
440 intensity were evaluated against the CDL-based results for twelve USDA-defined sub-regions in
441 the U.S. for the year 2016 (Table 5). Our results showed that user's accuracies were higher than
442 60% in ten regions, which varied from 60% to 93.67%. The producer's accuracies in seven regions
443 reached 60% except for the double-cropping system in Mountain, Pacific, and Southern Plains.
444 Seven regions had overall accuracies over 80%. Particularly, accuracies in three major agricultural
445 regions (Heartland, Upper Midwest, and Great Lakes) were higher than 85%. Relatively low
446 accuracies ($< 75\%$) were found in the Mountain, Northwest, and Pacific regions where agricultural
447 areas are generally more fragmented. For kappa coefficients, values ranged from 0.29 to 0.73, with
448 7/10 regions being over 0.55.

449 **Table 5** Accuracies (%) of Satellite-estimated Cropping Intensity in the U.S. for the year 2016.

Regions		Heartland	Mountain	Northern Plain	Northwest**	Pacific	Upper Midwest**
Single crop	PA*	96.83	82.63	77.35	-	87.10	-
	UA*	89.25	68.32	77.81	-	74.81	-
Double crop	PA	67.59	44.69	77.27	-	39.76	-
	UA	88.48	64.05	76.81	-	60.00	-
	OA*	89.09	67.11	77.31	71.97	71.60	88.05
	Kappa	0.70	0.29	0.55	-	0.29	-
Regions		Delta	Eastern Mountain	Great Lakes	Northeastern	Southern	Southern Plains
Single crop	PA	85.36	88.59	89.50	61.05	89.74	91.69
	UA	93.35	78.98	87.30	77.21	70.85	74.95
Double crop	PA	81.95	83.64	82.78	90.72	80.43	50.63
	UA	65.37	91.35	85.63	81.89	93.67	79.09
	OA	84.50	85.67	86.60	80.63	83.66	75.96
	Kappa	0.62	0.71	0.73	0.55	0.66	0.45

450 *Note.* * PA, UA, and OA represent the producer’s accuracy, user’s accuracy, and overall accuracy,
 451 respectively. **These two regions only have single cropping systems.

452 **3.2 Evaluation of the satellite-derived crop phenology**

453 Based on our estimated phenological stages, we calculated the dates of 80% (the U.S.) and 20% -
 454 100% (Canada) progress of crops and compared them against those from the crop reports (Table
 455 6 in the U.S. and Table 7 in Canada). Generally, the R^2 values were higher than 0.60, the RMSEs
 456 were lower than ten days, and the MAEs were lower than eight days for all predicted phenological
 457 stages, except for soybean in Canada ($R^2 = 0.35$). Our results demonstrated a relatively high
 458 accuracy for predicting the major crop phenological stages. In the U.S., evaluation results showed
 459 that more than half of the values of R^2 (13/24) were higher than 0.80. For sorghum in the U.S., all
 460 R^2 values were higher than 0.90, RMSEs were lower than five days, and MAEs were lower than

461 four days. For Canada, only three of ten R^2 values were lower than 0.70, all RMSEs were lower
462 than eight days, and MAEs were lower than seven days. Relatively higher accuracies were found
463 for corn ($R^2=0.99$) and soybean ($R^2=0.90$) harvesting dates in Canada compared to those in the
464 U.S. The relatively larger errors for soybean (planting dates) in Canada might be attributed to the
465 small sample sizes and different ground data acquisition methods.

466 Previous studies have reported differences between the remote sensing-based crop planting
467 estimations and those reported by ground observations. For example, Hmimina et al. (2013) found
468 the differences were 10.5 and 24.2 days between the crop phenological dates derived from the
469 MODIS daily and 16-day products, respectively. Ortiz-Monasterio and Lobell (2007) reported that
470 approximately one-week difference was found between the observed and estimated crop planting
471 dates. In this study, our results showed that the differences were lower than seven days between
472 the estimated planting dates and crop reports for all crop types, except the corn in the U.S. (7.62
473 days). It illustrated that the key points used for detecting crop planting dates could capture the
474 event well.

475 For each phenological stage of seven major crops, we plotted the time ranges of the satellite-based
476 crop phenological dates and ground recorded data (Appendix Figs. 2S A ~ E: The U.S., F, and G:
477 Canada, H and I: Mexico). For the U.S., some crop phenological stages were not included in the
478 comparisons because no records are available in the crop reports. Similarly, for Canada and
479 Mexico, we only analyzed planting and harvesting dates due to limited data availability. Our
480 evaluation results suggested that the satellite-based major crop phenological dates closely matched
481 those from the ground observation in the U.S. and Canada (Appendix Figs. 2S A~G). For Mexico,
482 the validation of planting dates and harvesting dates for corn and sorghum also exhibited a high
483 agreement with FAO recorded datasets. Over 80% of the predicted phenological dates were within

484 the recorded range of crop calendar datasets from FAO, except for the harvesting dates of corn
 485 (Appendix Figs. 2S H and 2S I).

486 **Table 6** Evaluation of the Satellite-estimated Phenological Stages in the U.S.

Stages	Statistics	Corn	Soybean	Spring wheat	Cotton	Barley	Sorghum
Planting	RMSE (days)	9.13	6.84	5.63	9.71	4.11	4.54
	MAE (days)	7.62	5.56	4.12	6.10	2.71	3.62
	R ²	0.65**	0.76**	0.87**	0.81**	0.85**	0.94**
	N	98	84	43	42	34	45
Jointing	RMSE (days)	-	-	5.6	6.19	-	-
	MAE (days)	-	-	5.33	4.58	-	-
	R ²	-	-	0.96**	0.60**	-	-
	N	-	-	6	43	-	-
Heading	RMSE (days)	5.42	8.50	5.58	8.29	3.03	4.95
	MAE (days)	4.42	7.41	4.42	6.26	2.32	3.73
	R ²	0.77**	0.65**	0.80**	0.63**	0.93**	0.96**
	N	110	79	45	43	34	45
Mature	RMSE (days)	6.26	4.70	6.10	-	-	5.03
	MAE (days)	5.18	3.98	4.75	-	-	3.56
	R ²	0.81**	0.71**	0.63	-	-	0.97**
	N	111	83	4	-	-	45
Harvesting	RMSE (days)	6.48	8.11	7.56	3.75	9.52	4.42
	MAE (days)	4.91	6.50	6.37	3.04	8.26	3.42
	R ²	0.77**	0.66**	0.80**	0.88**	0.79**	0.96**
	N	110	83	38	45	27	45

487 *Note.* N represents the number of states or provinces used for evaluation. ** represents a 1%
 488 significance level

489

490

Table 7 Evaluation of the Satellite-estimated Phenological Stages in Canada.

Stages	Statistics	Corn	Soybean	Spring wheat	Barley	Canola
Planting	RMSE (days)	6.94	7.71	4.68	5.58	6.03
	MAE (days)	6.20	6.70	3.75	4.56	5.18
	R ²	0.72*	0.35*	0.77**	0.77**	0.63**
	N	10	10	12	18	22
Harvesting	RMSE (days)	4.42	6.36	3.45	7.88	6.22
	MAE (days)	3.50	4.50	3.00	6.5	5.15
	R ²	0.99*	0.90*	0.75**	0.62**	0.84**
	N	4	6	11	16	20

491 *Note.* N represents the number of states or provinces used for evaluation. * represents a 5%
492 significance level.** represents a 1% significance level.

493 3.3 Comparison with existing datasets and studies

494 We evaluated our results against crop planting and harvesting dates from two previous studies.
495 The Crop Calendar Dataset provides *in situ* observations of crop planting and harvesting dates
496 derived from FAO and USDA census in 2007 and 2008 (Sacks et al., 2010). The SACRA (the
497 SATellite-derived CRop calendar for Agricultural simulations) dataset represents the estimated
498 global sowing and harvesting dates based on the time series of averaged VEGETATION/SPOT
499 NDVI during 2004 - 2006 (Kotsuki and Tanaka, 2015).

500 Our comparisons (Tables 8 and 9) suggested that our estimated planting dates were slightly later
501 than the Crop Calendar Dataset in 19 of the total 23 states considered in the comparison, while the
502 harvesting dates were relatively earlier in 12 states. In most states, discrepancies between our
503 estimated planting dates or harvesting dates and those from the Crop Calendar Dataset were less
504 than 15 days (Table 8). Crop Calendar Dataset was digitized from ground observations derived

505 from several different resources, most of which were specified for an entire country or a sizeable
506 sub-national unit (e.g., a single state in the US). Lacking valuable spatial information of crop
507 phenology could limit the application of the dataset at the regional or landscape scales. Moreover,
508 the dataset does not capture any phenological changes in time, which only refers to planting and
509 harvesting dates for the 1990s or early 2000s. The comparison between our estimates with the
510 SACRA suggested large discrepancies in both planting dates/harvesting dates; in particular, three
511 crop types except for spring wheat displayed large differences in planting dates in North Dakota
512 (Table 9). This could be partly attributed to the fact that the SACRA dataset only selected one
513 dominant crop in each administrative unit. Moreover, it was produced using the time series of the
514 NDVI averaged from three consecutive years (2004 – 2006) at a resolution of 5 arcmin. We further
515 compared our estimated planting and harvest dates with those from the SACRA at the state level
516 using the USDA crop reports for the period 2004-2006 (Appendix Table S3). The results showed
517 that our estimates (RMSEs and MAEs lower than 15 days) had a better performance than the
518 SACRA (RMSEs and MAEs were larger than 22 and 12 days, respectively).

519 Besides, to verify the robustness of our improved approach, we also compared our results with the
520 phenological stages derived from the same key points but without setting thresholds. Higher
521 accuracies were found for the estimations of all crop types detected from the improved EVI-curve-
522 based approach (Appendix Table S4).

523

524

525

526 **Table 8** Comparison of the Estimated Planting and Harvesting Dates versus Sacks et al. (2010) at
 527 the state level.

States	Crop types	Planting date (DOY)		Difference (days)	Harvesting date (DOY)		Difference (days)
		Results (2007-2008)	Sacks et al. (2010)	Results (2007-2008) – Sacks et al.(2010)	Results (2007-2008)	Sacks et al. (2010)	Results(2007-2008)–Sacks et al.(2010)
IL	Corn	151	130	21	295	295	0
MN	Corn	149	136	13	296	302	-6
NE	Corn	149	131	18	291	299	-8
MI	Corn	136	136	0	285	306	-21
CO	Corn	145	128	17	287	304	-17
AR	Corn	123	119	4	263	256	7
IN	Corn	148	138	10	292	303	-11
KS	Corn	130	122	8	274	281	-7
MO	Corn	139	128	11	282	289	-7
ND	Corn	146	139	7	291	292	-1
OH	Corn	146	137	9	293	298	-5
SD	Corn	145	141	4	290	300	-10
NC	Corn	111	115	-4	241	271	-30
TX	Corn	93	97	-4	232	251	-19
IA	Soybean	165	146	19	304	282	22
MI	Soybean	169	147	22	305	292	13
IL	Soybean	149	147	2	297	286	11
IN	Soybean	161	148	13	297	289	8
OH	Soybean	165	150	15	305	289	16
MN	Soybean	165	150	15	301	286	15
WI	Soybean	157	153	4	301	294	7
NE	Soybean	161	158	3	305	291	14
MO	Soybean	169	158	11	309	298	11
MAE (days)				10.17			11.57
RMSE (days)				12.00			13.46

528 *Note.* The comparison focused on 2007-2008, consistent with the study period in Sacks et al. (2010).

529 **Table 9** Comparison of the Estimated Planting and Harvesting Dates versus SACRA at the state
 530 level.

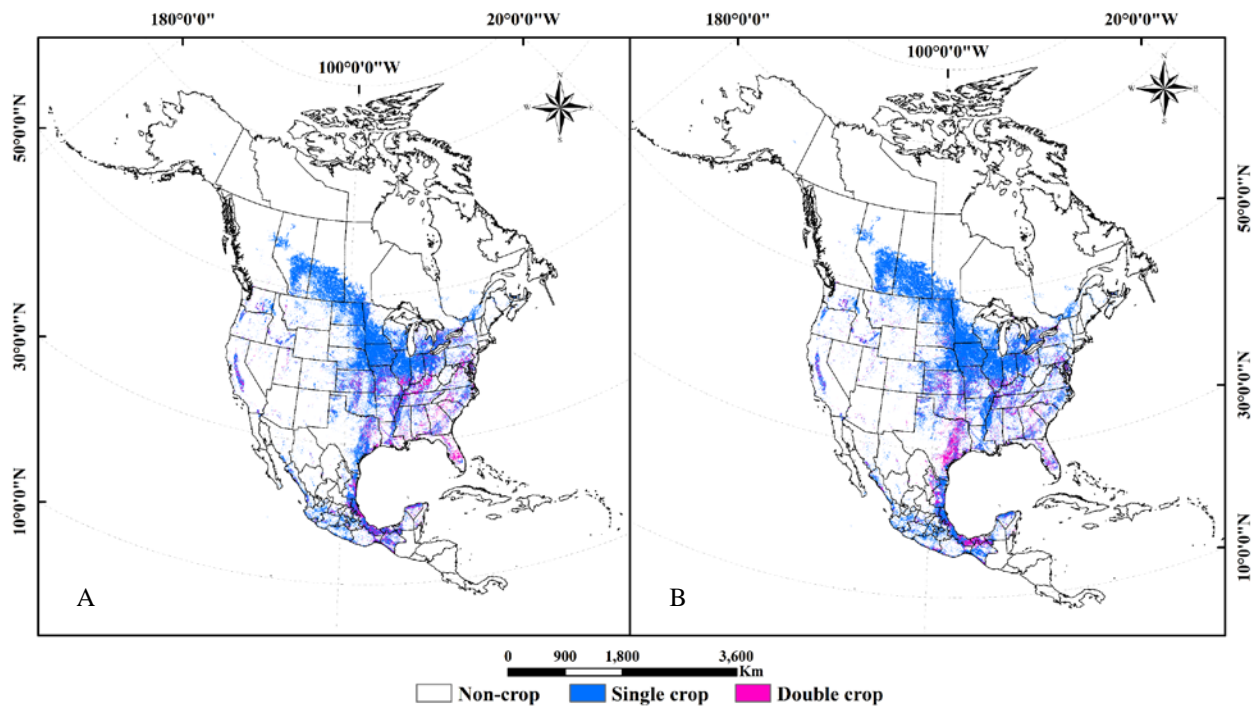
States	Crop types	Planting date (DOY)		Difference (days)	Harvesting date (DOY)		Difference (days)
		Results (2004-2006)	SACRA	Results (2004-2006) - SACRA	Results (2004-2006)	SACRA	Results (2004-2006) - SACRA
IL	Corn	140	82	58	284	249	35
MN	Corn	149	98	51	296	259	37
NE	Corn	146	95	51	291	243	48
MI	Corn	136	108	28	285	264	21
AR	Soybean	139	80	59	280	264	16
IN	Soybean	146	99	47	287	262	25
MO	Soybean	136	92	44	283	253	30
OH	Soybean	148	118	30	290	257	33
SD	Soybean	146	110	36	292	263	29
NC	Soybean	131	91	40	277	299	-22
SC	Soybean	125	93	32	273	307	-34
MS	Soybean	126	87	39	271	299	-28
LA	Soybean	123	83	40	265	293	-28
ND	Spring wheat	127	144	17	267	234	33
GA	Cotton	138	79	59	299	329	30
MAE (days)				42.07			29.93
RMSE (days)				39.92			28.13

531 *Note.* The comparison focused on 2004-2006, consistent with the study period in Kotsuki and
 532 Tanaka (2015).

533 3.4 Spatial and temporal patterns in cropping intensity

534 The satellite-based cropping intensity map showed evident spatial patterns in North America (Fig.
 535 3). The agriculture in North America was dominated by the single-cropping system during the
 536 study period, which mainly occurred in Canada and the northern U.S. The double cropping system
 537 was primarily distributed in Mexico, the southern U.S., and parts of the southeastern U.S. Single-

538 cropping system dominated in Canada and was relatively stable during 2000 - 2016. There were
539 no noticeable spatial transitions of cropping intensity in Mexico during the study period.
540 Only two years of the results are presented, but the general patterns of cropping intensity remained
541 roughly constant throughout the study period, although an expansion of double-cropping areas was
542 found in the lower Great Plains.



544 **Fig. 3.** Distribution of the single and double-cropping systems across North America in 2000 (A)
545 and 2016 (B).

546 Table 10 showed the results of the Mann-Kendall test and Sen's slop of cropping intensity in North
547 America. A significant increasing trend was detected in the single cropping system with a rate of
548 5,489,000 acres per year at the 1% significance level. However, no significant trend was found for
549 the double-cropping system.

550
551

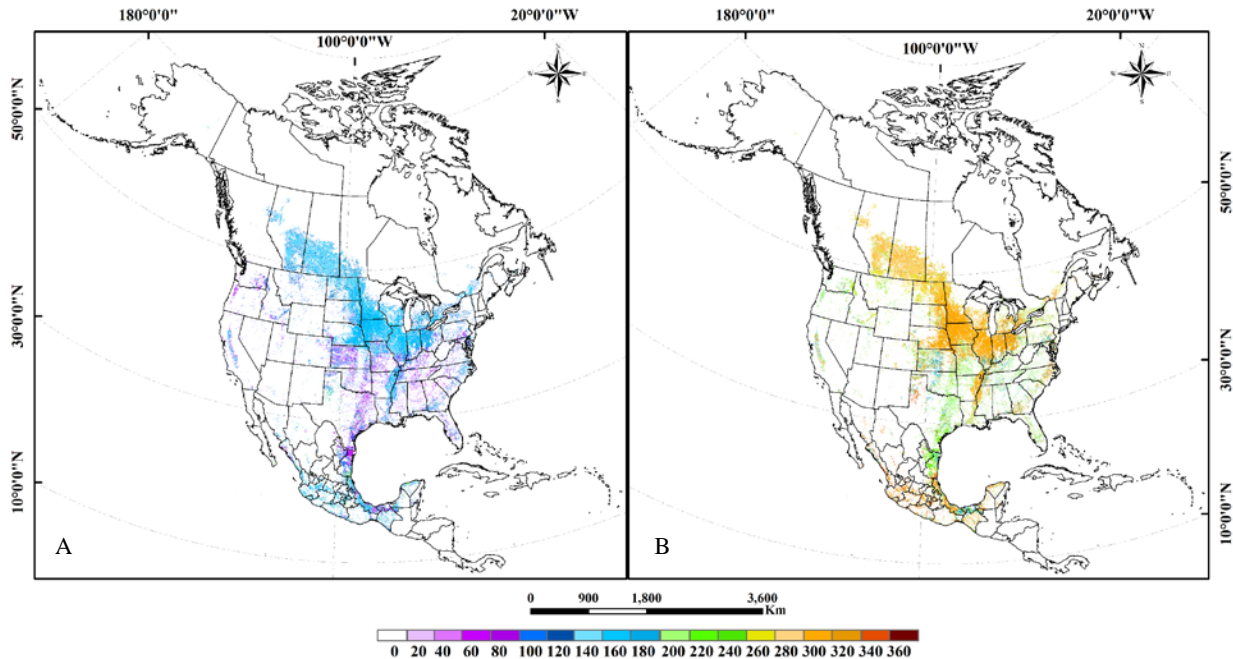
552 **Table 10** Temporal trends of cropping intensity using Mann-Kendall test

Crop rotation	Test	
	Mann-Kendall test (Z)	Sen's slop (*1,000 acres)
Single crop	2.68	5,489*
Double crop	-0.29	-1,432

553 *Note.* * represents a 1% significance level

554 3.5 Spatial and temporal patterns in crop planting and harvesting dates

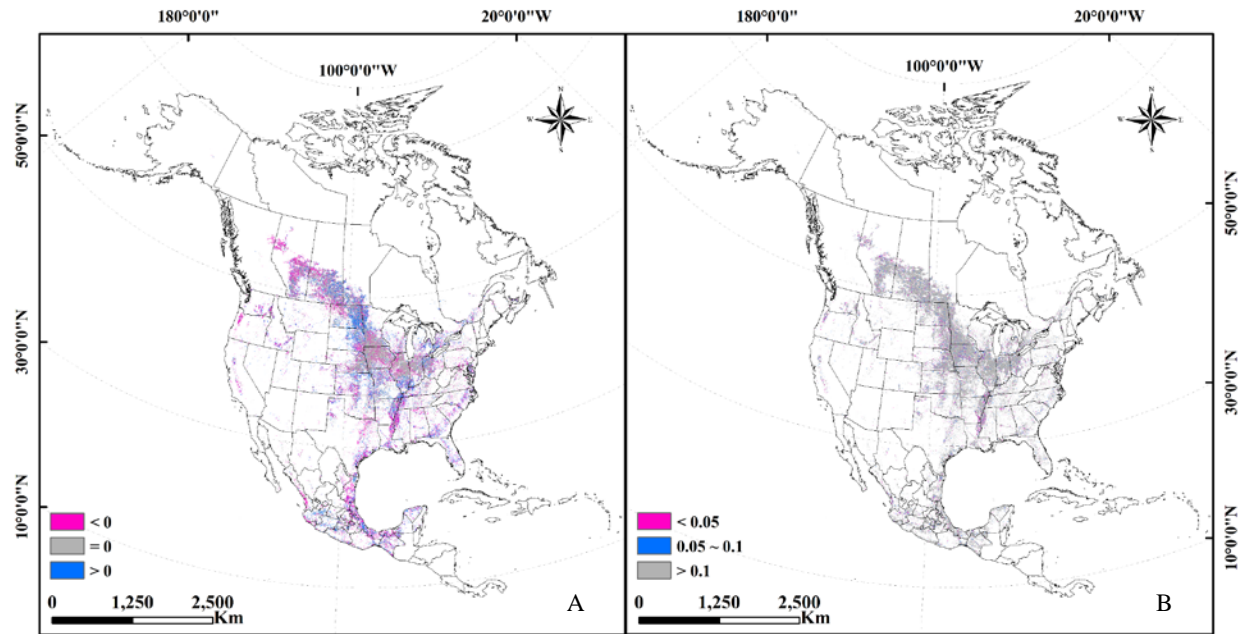
555 The spatial patterns of planting and harvesting dates in the single-cropping system and the first
556 season of the double-cropping system for the year 2016 were shown in Fig. 4. Spatially, the crop
557 planting dates in the northern areas of North America (e.g., Canadian Prairies, the north of the US
558 Midwest and Great Plain) were generally later than those in most of the southern regions. The
559 planting dates showed a slightly increasing trend with latitudinal gradients between 20°N and 70°
560 N latitude (Fig. 4A). The estimated results for crop harvesting dates showed a similar spatial trend
561 to that of the planting dates, which later harvesting dates occurred in the Canadian Prairies, much
562 of the US Midwest and parts of the northern Great Plain (Fig. 4B). This phenological trend in
563 planting and harvesting dates characterized the spatial variability in geographic patterns and might
564 be explained by climatic temperature and distributions of different crop types. In most croplands
565 of Mexico, the crop planting dates generally began from 140 to 180 (Julian Day), and harvesting
566 dates mainly fell into the range of 280 to 320 (Julian Day).



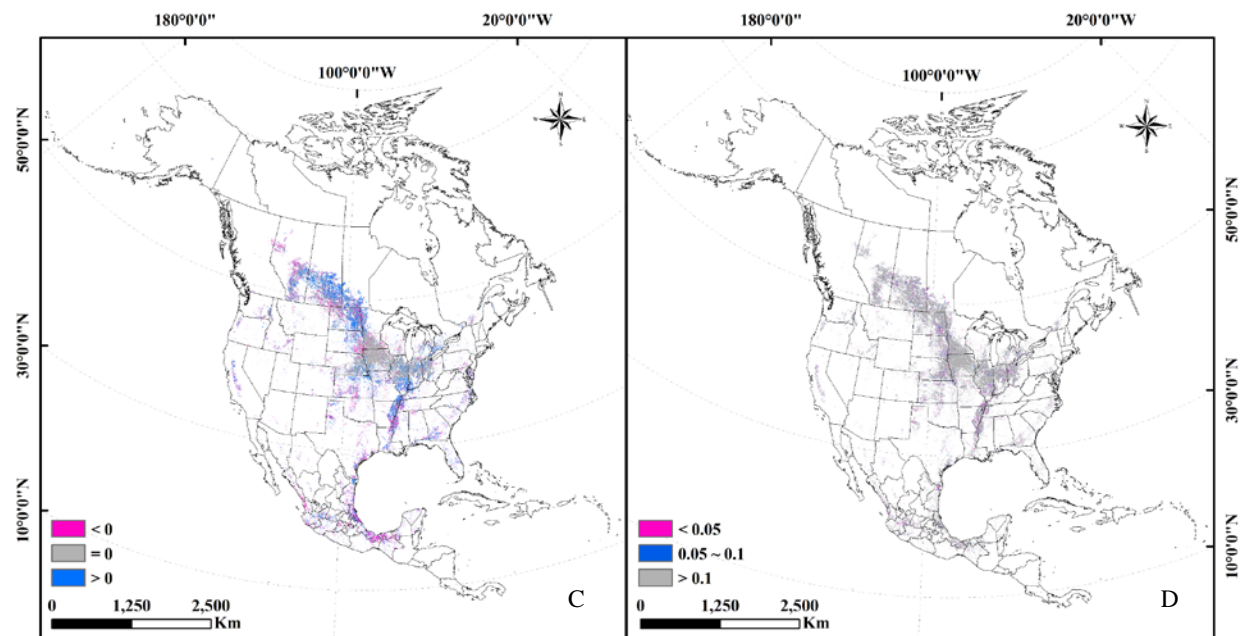
567

568 **Fig. 4.** Estimated planting dates (A) and harvesting dates (B) of the first growing season across
 569 North America in 2016.

570 We further performed a temporal trend analysis for crop planting/harvesting dates (Fig. 5) and
 571 summarized in Fig. 6. Sen’s slope represents the changing trends during the study period in Fig. 5.
 572 For the planting dates, approximately half of the evaluated pixels showed negative trends, less than
 573 a quarter showed positive trends, and the rest of the areas showed no significant trends. The pixels
 574 with advanced planting dates were sparsely distributed across North America. For harvesting dates,
 575 the areas with delayed trends were mainly clustered in the mid and high latitudes of North America.
 576 In particular, croplands in Canadian Prairies and the north of the Mississippi River in the U.S.
 577 showed delayed harvesting dates. However, only approximately 10% ($p < 0.1$) of the evaluated
 578 areas over North America witnessed significant changes in both planting and harvesting dates
 579 during the period 2000 - 2016.

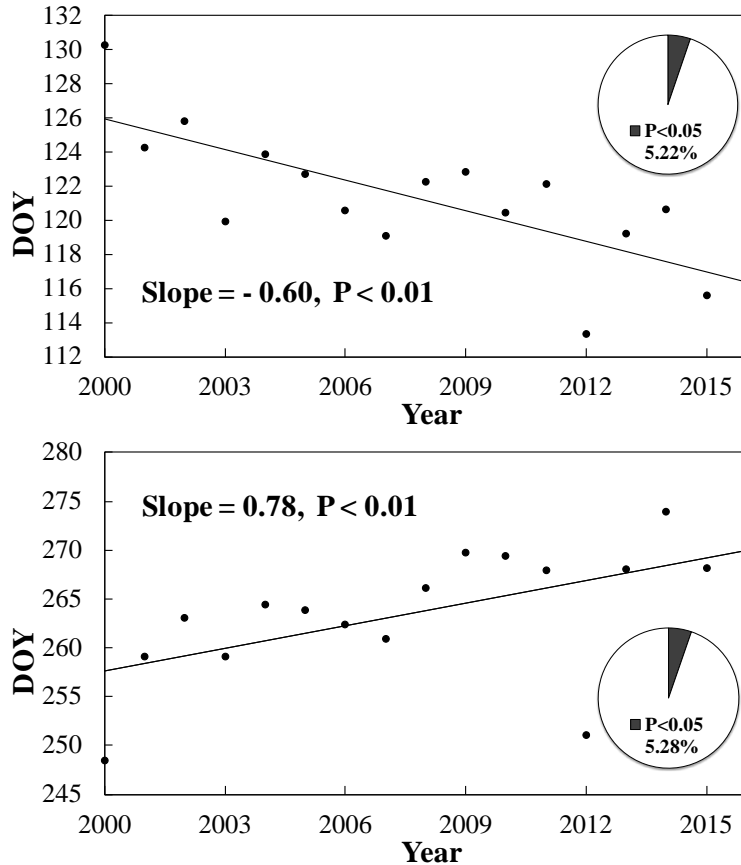


580



581

582 **Fig. 5.** Mean-Kendal trend tests for the planting (A: Slope, B: P values) and harvesting dates (C:
 583 Slope, D: P values) of the first growing season across North America (Slope: change rate of crop
 584 phenological dates; P values: the confidence of trend analysis; The slope values lying outside the
 585 95% confidence intervals were not included in the statistics; pixels with less than 12 years being
 586 identified as cropland, which were not included in the Mann-Kendall statistical test).



587

588 **Fig. 6.** Changing trend of averaged planting dates (A) and harvesting dates (B) in North America
 589 ($p < 0.05$) (pixels that were identified as cropland for less than 12 years were not included in the
 590 Mann-Kendall statistical test).

591 To investigate the crop phenology trends at the continental scale, we first separately computed the
 592 spatial averages of planting and harvesting dates and then fitted their changing patterns during the
 593 study period (Fig. 6). For the areas with significant changes, we found that the planting dates of
 594 the first growing season advanced by 0.60 days/year ($p < 0.01$), or about 10.20 days over the entire
 595 study period. For the harvesting dates in areas with significant trends, our results suggested a
 596 delaying trend at a rate of 0.78 days/year ($p < 0.01$), i.e., 13.26 days over the entire study period.
 597 We further divided entire North America into 14 sub-regions, including Canada, Mexico, and
 598 twelve regions of the U.S. (Appendix Table S2, Fig. S3). Of the 14 sub-regions, 11 experienced
 599 an advancement in the planting dates during the study period, which accounted for 72.5% of the

600 total areas with statistically significant changes; 9 sub-regions postponed in harvesting dates,
601 accounting for 75.5% of the total areas with statistically significant changes (Appendix Fig. S3).
602 Regionally, the northern and eastern parts of North America were found to have experienced the
603 most significant delays in crop harvesting dates.

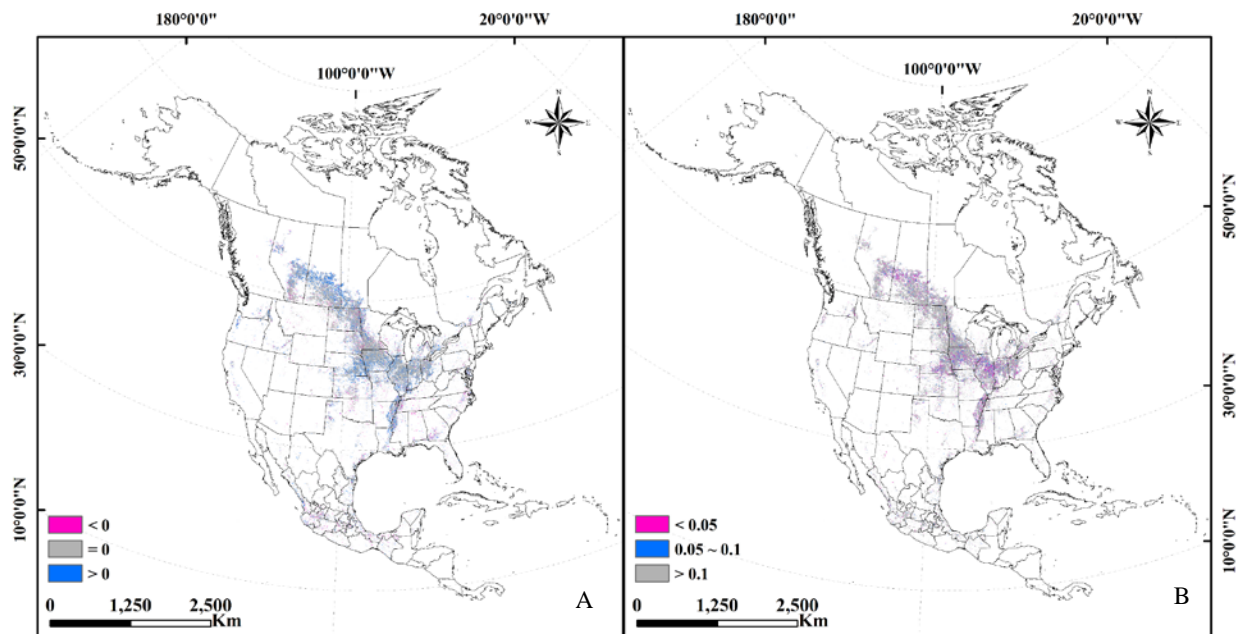
604 **3.6 Climate change impacts on crop phenology**

605 **3.6.1 Temporal trend analysis of crop growing season length based on thermal zones**

606 Fig. 7 displays the spatial distribution of the changing trends of crop growing season length as
607 calculated from the planting and harvesting dates during the study period. Positive values (blue)
608 and negative values (red) represent the prolonged growing season and shortened growing seasons,
609 respectively. During the study period, the averaged crop growing seasons have extended at a rate
610 of 0.33 days/year ($P < 0.01$) over North America. The extension of crop growing seasons is mainly
611 concentrated in the U.S. and Canada ($> 30^{\circ}\text{N}$) with higher significance (Fig. 7). In contrast, most
612 areas of Mexico ($< 30^{\circ}\text{N}$) indicated shortened crop growing seasons. In addition, areas with
613 extended growing seasons (slope > 0) displayed a gradual increase along with increasing latitude
614 in North America (Fig. 7A).

615 Based on the Global Agro-ecological Zones (GAEZ v3.0, <http://www.fao.org/nr/gaez/en/>)
616 (Appendix Fig. S5), we further performed a trend analysis to characterize the temporal variations
617 in the length of the crop growing season. North America is classified into 12 zones in the GAEZ
618 v3.0, and the cropland areas fall within six of them. In this study, we regrouped two tropics into
619 the region a, four subtropics into the region b, three temperate zones into the region c (Appendix
620 Fig. S6). We excluded the year 2000 in the trend analysis because of the incomplete MODIS EVI
621 time series. The analysis showed various temporal patterns in the crop growing season length
622 among eco-regions in North America during the study period. Shortened crop growing seasons

623 were mainly found in tropics (slope = - 0.146, $P < 0.01$), while significantly extended crop growing
624 seasons occurred over the subtropics (0.48 days/year) and temperate zones (0.65 days/year).



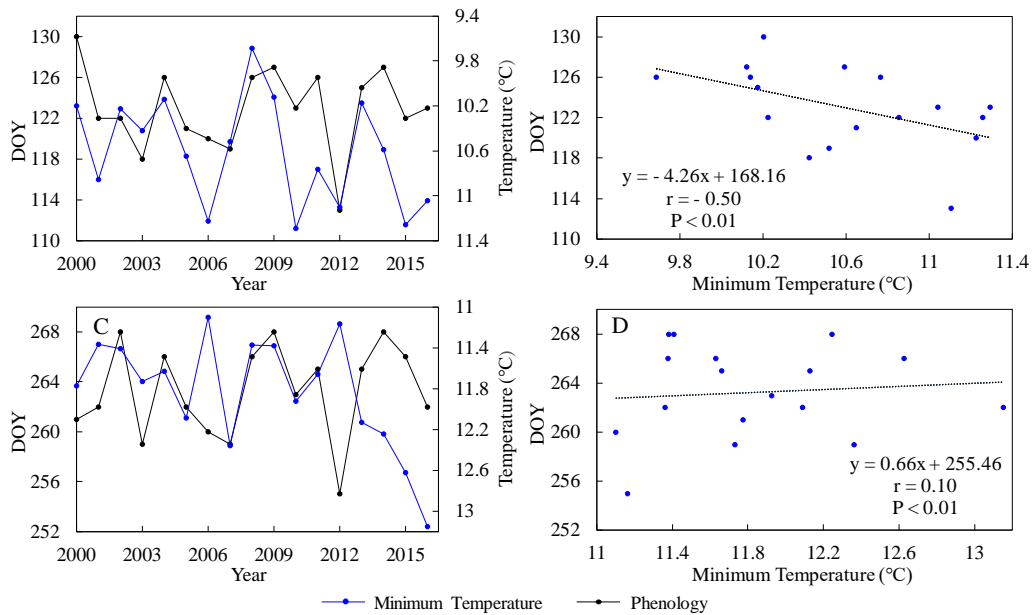
625
626 **Fig. 7.** Mean-Kendal trend tests for the crop growing season (A: Slope, B: P values) across North
627 America (pixels identified as cropland for less than 12 years were not included in the Mann-
628 Kendall statistical test).

629 3.6.2 Correlations between crop phenology and climatic factors

630 Our climate analysis suggested that, at the continental scale, planting dates had a negative
631 correlation with the average daily minimum/maximum temperatures during the crop sowing
632 season (minimum temperature: $r = - 0.50$, $p < 0.01$; maximum temperature: $r = - 0.62$, $p < 0.01$).

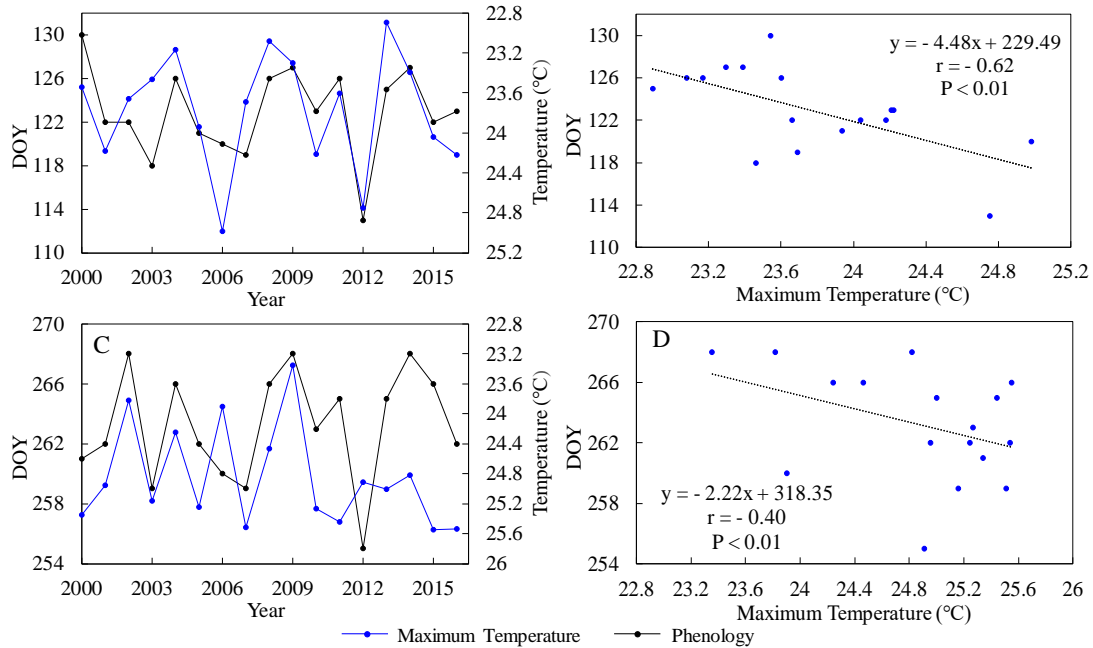
633 An increase of 1°C in average daily minimum/maximum temperatures from April to June resulted
634 in an advancement of 4.26/4.48 days in crop planting dates (Figs. 8, 9, and 10). For the harvesting
635 dates, our results suggested that an increase of 1°C in minimum temperature during August through
636 October resulted in a delay of 0.66 days ($r = 0.10$, $P < 0.01$); while an increase of 1°C in maximum
637 temperature during the same period resulted in an advancement of 2.22 days ($r = - 0.40$, $P < 0.01$).

638 Correlation analysis for the other three phenological stages (jointing, heading, and maturity dates)
 639 and climatic temperature can be found in Appendix Figs. S7 and S8. Over the study period,
 640 significant negative correlations were found between three crop stages (jointing, heading, and
 641 maturity dates) and average daily maximum temperature. Two of three stages (jointing and
 642 heading dates) showed advanced trends with the increasing average daily minimum temperature.



643

644 **Fig. 8.** Interannual changes in estimated planting and harvesting dates and average daily
 645 minimum temperatures for planting (A, B: April to June) and harvesting seasons (C, D: August
 646 to October) in North America during 2000-2016.



647

648 **Fig. 9.** Interannual changes in estimated planting and harvesting dates and average daily
 649 maximum temperatures for planting (A, B: April to June) and harvesting seasons (C, D: August
 650 to October) in North America during 2000-2016.

651 **4. Discussion**

652 **4.1 Satellite-based crop phenology approach**

653 Satellite imagery has been widely used for crop phenology monitoring over the past decades
 654 (Boschetti et al., 2009; Chmielewski et al., 2004; Hmimina et al., 2013). The NDVI is one of the
 655 vegetation indexes for extracting crop phenology. For example, You et al. (2013) used a threshold-
 656 based method and the AVHRR NDVI time series for identifying the start and end of the growing
 657 season for 43 different agricultural zones in China. Zheng et al. (2016) produced a synthetic NDVI
 658 time series fused from SPOT 5 and MODIS to extract crop phenology over areas with high
 659 fragmented farmlands. However, the NDVI application is limited by its tendency to saturate at
 660 high canopy density and coverage (Bausch, 1993). When the crops reach canopy closure, the
 661 NDVI also tends to saturate (Rouse et al., 1974) and produce inaccurate estimates of crop

662 phenology, especially for crop heading date detection (Son et al., 2014). Also, the NDVI is very
663 sensitive to soil background effects at incomplete vegetative cover conditions, which may bring
664 more uncertainties in the early stage of crop growth when the LAI is still low (Huete et al., 1988).
665 In contrast, EVI is constructed by decoupling the canopy background signal and reducing
666 atmospheric influences, which can overcome the saturation and soil noise problems of NDVI
667 (Huete et al., 1997). Using the smoothed EVI time series, Sakamoto et al. (2005) proposed the
668 wavelet transform-based method to retrieve the rice planting, heading, and harvesting dates in
669 Japan successfully. But the mother wavelet and the threshold used for determining each
670 phenological stage vary with regions and crop species, limiting the method's application for other
671 crops and over large areas.

672 Generally, remote-sensing-based approaches to detect plant phenology can be classified into two
673 general categories, i.e., threshold-based methods and VI change detection methods (Zeng et al.,
674 2020). Threshold-based methods use identical thresholds to determine crop phenological stages in
675 all cropping systems. For example, Delbart et al. (2005) adopted 20% of the NDVI amplitude to
676 estimate senescence dates of both croplands and natural vegetation types. White et al. (1997) used
677 50% of the NDVI amplitude to determine the start and end of the season. Threshold-based methods
678 may generally describe changing patterns of crop phenology, but cannot catch discrepancies
679 among various crops and different cropping systems (Huang et al., 2019). VI change detection
680 methods retrieve the crop phenological dates through detecting the changing characteristics of the
681 VI time series curve, such as some key points in the VI and the first derivative of VI or the changing
682 rates of curvature (Zeng et al., 2020). VI change detection method was considered an effective
683 way to extract the phenological metrics for general vegetation types. For example, Sakamoto et al.
684 (2010) used a Two-Step Filtering method to analyze the changing characteristics of VI curves and

685 detect the specific phenological dates of corn and soybean in eastern Nebraska. However, changing
686 characteristics derived from VI profile might be sensitive to non-vegetation-related variations such
687 as noise components caused by aerosols and bidirectional reflectance distribution or other climatic
688 factors, resulting in significant uncertainties in the phenology timing estimates. Besides,
689 complicated crop planting patterns, such as double or multiple cropping systems, make the crop
690 phenology detection more difficult over the large area (Ogle et al., 2005).

691 In this study, we combined the advantages of both threshold-based and VI change detection
692 methods by using specific key points of EVI curves and its first/second derivatives, along with the
693 dynamic thresholds to confine the ranges of each stage. We expanded to quantifying five main
694 crop phenological phases (i.e., the dates of planting, jointing, heading, maturity, and harvesting)
695 of seven major crop types over North America during 2000-2016. Compared with the VI change
696 detection method without setting thresholds, our improved approach showed better performances
697 (Appendix Table S4). The estimated crop phenological stages also demonstrate a more favorable
698 agreement with ground information than previous studies (Section 3.3).

699 **4.2 Changing trends in crop phenology**

700 The temporal and spatial variations in crop phenology have been widely investigated in previous
701 studies. Spatially, many studies indicated a latitude-dependent changing pattern in crop phenology,
702 particularly in mid and high Northern Hemispheres (Chmielewski et al., 2004; Liu et al., 2017;
703 Luo et al., 2020; Yu et al., 2012). Our spatially explicit results confirmed these findings by showing
704 a slightly increasing trend in planting and harvesting dates with latitudinal gradients from 20° to
705 70°N in North America (Fig. 4). Crop phenology in Mexico did not exhibit a latitudinally changing
706 pattern. It might be partially attributed to the non-obvious latitudinal gradient of temperature in

707 the tropical region (Ogle et al., 2005), different cropping systems (Hansen et al., 2016), and other
708 factors related to management practices (Martin et al., 2005).

709 As for temporal variations, many studies have reported that some crop phenological stages, such
710 as planting and harvest dates, had either delayed or advanced over recent decades. For example,
711 an analysis of observations from phenological network stations showed earlier corn planting dates
712 (0.17 days/year) in Germany from 1961 - 2000 (Chmielewski et al. 2004). Using long-term VI
713 time series, Wang et al. (2017) observed an advance in spring green-up date for winter wheat (0.18
714 days/year) in North China Plain over the period 1982 - 2013. Sacks and Kucharik (2011) reported
715 advanced planting trends (0.40 days/year for corn and 0.50 days/year for soybean) in the U.S.
716 during 1981 - 2005. Zhu et al. (2012) observed the delayed dormancy (0.55 days/year) during 1982
717 - 2006, with mean rates averaged by natural vegetation and crops in North America. These studies
718 are limited by either specific crop types or phenological stages, with few at large scales and over
719 long time series. In this study, we derived spatially explicit five crop phenological stages of seven
720 crop types at the North America continental scale. Our estimated changes in planting and
721 harvesting dates fall within the reasonable range compared to previous studies, despite slightly
722 more apparent changing rates (Section 3.5, Fig. 6) due to different data sources and study periods.

723 Our spatially explicit estimates of multiple phenological stages for seven major crops provide more
724 detailed information for crop yield prediction and climate change assessments at large scales.

725 The length of growing season may have significant effects on seasonal variations in carbon, water,
726 and nutrient processes as well land surface energy balance, therefore have implications for crop
727 security and terrestrial biogeochemical cycles. Several studies have suggested the extended or
728 shortened period for various crop types in different regions. For example, Chen et al. (2012) found
729 that the growth durations of rice, corn, and soybean in Northeast China have prolonged by 14 days,

730 7.0 days, and 2.7 days since the 1950s, respectively. Sacks and Kucharik (2011) presented that the
731 crop growth period in the U.S. has been longer by 0.50 days/year for corn and 0.31 days/year for
732 soybean from 1981 - 2005. Our study also reported a prolonged crop growing season length,
733 especially in the temperate and subtropical areas (Section 3.6.1, Fig.7 and Appendix Fig. S6). Our
734 extended crop growing period is well supported by some previous studies based on the intensive
735 ground observations (Tao et al., 2014; Zhang et al., 2014) and regional estimations (Peltonen-
736 Sainio et al., 2009). The concurrent of advanced planting and delayed harvesting contributes to the
737 prolonged crop growing seasons in North America. The crop variety shift aiming to improve crop
738 production may also extend the growing season (Tao et al., 2012; Wang et al., 2013; Wang et al.
739 2018). In addition, irrigation, intensive management practices such as reduced or zero-till, cover
740 crop, and fertilizer use have been significantly improved during the last several decades, which
741 may have positively affected crop phenology development (He et al., 2015).

742 **4.3 Crop phenology in correlation with climate factors**

743 Previous studies have indicated that climate changes have promoted variations in vegetation
744 phenology (Oteros et al., 2015; Sacks et al., 2010; Sparks et al., 2005; Wang et al., 2016).
745 Temperatures have been regarded as the primary control of vegetation phenological progress
746 (Badeck et al., 2004; Piao et al., 2019). The distinct responses of crop phenology to temperatures
747 in the spring or autumn season were reported in many studies (e.g., He et al., 2015; Kucharik et
748 al., 2006; Tao et al., 2014; Zhang et al., 2019). Some studies found that temperature changes had
749 led to appreciable responses in crop phenology in many parts of the Northern Hemisphere. For
750 example, Tao et al. (2006) analyzed observations on agro-meteorological stations and found that
751 the planting dates of corn were significantly related to the spring temperatures during 1981–2000,
752 with an advance of 2.12 days and 2.28 days for each 1 °C rise in minimum and maximum

753 temperatures, respectively. Chmielewski et al. (2004) showed that an increase of 1°C in average
754 temperatures between February and April led to an advanced beginning of the growing season of
755 fruit trees and crops by 4.7 days in Germany from 1961 to 2000. Our study confirmed these
756 findings and suggested that an increase of 1°C in average daily minimum/maximum temperatures
757 from April to June might have resulted in an advancement of 4.26 - 4.48 days in crop planting
758 dates. Accordingly, an increase of 1°C in average daily minimum/maximum temperature from
759 August to October might have resulted in a delay of 0.66 days or advancement of 2.22 days in crop
760 harvesting dates in North America during the study period.

761 Vegetation growth in mid-high latitudes of the North Hemisphere is particularly sensitive to
762 temperature changes in spring (Nemani et al. 2003; Slayback et al. 2003; Piao et al., 2019;
763 Schwartz et al., 2006). This is consistent with our results, showing more evident changes in the
764 planting dates than the harvesting dates in response to temperature changes. When investigating
765 spatial patterns, our results displayed both advances and delays occurring across the crop areas
766 (Fig. 5) in response to highly diverse climatic conditions. This finding agrees with Schwartz et al.
767 (2006), which also found spatially heterogeneous of the start of season across North America.

768 **4.4 Uncertainties and future needs**

769 In this study, we predicted spatial and temporal patterns in major crop phenological stages using
770 an improved EVI-curvature-based approach. We acknowledge uncertainties potentially derived
771 from the input data and the approach we used. First, we only used the 2005 and 2010 North
772 American land use and cover datasets because annual land cover maps were not available for entire
773 North America; this might bring some uncertainties to identifying crop phenological stages.
774 Second, the winter wheat is generally planted in late autumn and enters the dormant period before
775 the next year; its EVI curves tend to show two peaks due to the over-wintering stages, which may

776 result in biased identification of the planting dates. Third, we detected the harvesting date of the
777 first season as the planting date of the second season. We acknowledge this scheme may not work
778 for all situations and could be improved when more detailed phenology information for the double
779 cropping system is available. Forth, the perennial grasses were included in the classification of
780 cropland in this study; in this case, most parts of the forage grass with two harvest seasons were
781 identified as double cropping systems, which might result in over-estimation of the distribution of
782 double crops. Moreover, the estimated crop phenological stages might have relatively higher
783 uncertainties over areas with more fragmented croplands due to the effects of mixed and perimeter
784 pixels at a 500 m spatial scale. In addition, the prolonged crop growing season might be
785 overestimated because pasture or forage grass was difficult to separate from cropland in phenology
786 identification at coarse spatial scales. In the next step, phenological dates of winter wheat crop
787 should be included as more crop-specific distribution maps are available. Data fusion of high-
788 resolution satellite imagery is needed for reducing uncertainties in fragmented areas where mixed
789 cropland pixels are dominant. More ground observations and long-term time series crop-specific
790 maps will booster the accuracy of crop phenology identification.

791 **5. Conclusions**

792 This study quantified spatio-temporal patterns in five phenological stages of seven crop types
793 across North America from 2000 - 2016 based on the MODIS EVI time series data. The estimated
794 cropping intensity and phenological stages agree favorably with those observed from field surveys,
795 satellite-based maps, and results from other studies. Our results demonstrated that the improved
796 approach is capable of realistically capturing changing patterns in crop phenology at large scales.
797 This approach overcomes the overfitting flaws of the polynomial function at the start and end of
798 the growing season. It can be applied to other regions where no substantial site-level field

799 observations for parameterization and validation available. To the best of our knowledge, this
800 study offers the first attempt to provide spatially explicit time series information of five major crop
801 phenological dates with a moderate spatial resolution at the continental scale. Our study sheds light
802 on how the crop phenology spatially responded to climate change. The derived crop phenological
803 datasets can be used to drive process-based crop or ecosystem models for large-scale crop yield
804 prediction and biogeochemical dynamics assessment, and inform more resilient development
805 strategies.

806 **Acknowledgments**

807 This work was supported by the National Institute of Food and Agriculture, U.S. Department of
808 Agriculture (NIFA-USDA Hatch project 2352437000), and NASA Kentucky under NASA award
809 (number NNX15AR69H). The work by L. Ji was performed under USGS Contract
810 140G0119C0001. JBF contributed to this research at the Jet Propulsion Laboratory, California
811 Institute of Technology, under a contract with the National Aeronautics and Space Administration.
812 California Institute of Technology. Government sponsorship acknowledged. JBF was supported
813 in part by NASA IDS, CMS, and INCA programs. We thank Dr. Sanath Sathyachandran for
814 reviewing the manuscript and providing valuable comments. Datasets derived from this study will
815 be made available on the website. The authors declare no conflicts of interest.

816 Any use of trade, firm, or product names is for descriptive purposes only and does not imply
817 endorsement by the U.S. Government.

818 **References**

- 819 Atkinson, P.M.; Jeganathan, C.; Dash, J.; Atzberger, C., 2012. Inter-comparison of four models for
820 smoothing satellite sensor time-series data to estimate vegetation phenology. *Remote Sens.*
821 *Environ.* 123, 400-417. <https://doi.org/10.1016/j.rse.2012.04.001>
- 822 Badeck, F.W., Bondeau, A., Böttcher, K., Doktor, D., Lucht, W., Schaber, J., Sitch, S., 2004. Responses
823 of spring phenology to climate change. *New Phytol.* 162, 295-309. <https://doi.org/10.1111/j.1469-8137.2004.01059.x>
- 824
825 Bai, H., Xiao, D., 2020. Spatiotemporal changes of rice phenology in China during 1981–2010. *Theor*
826 *Appl Climatol.* 140, 1483–1494. <https://doi.org/10.1007/s00704-020-03182-8>
- 827 Bausch, W.C., 1993. Soil background effects on reflectance-based crop coefficients for corn. *Remote*
828 *Sens. Environ.* 46 (2), 213–222. [https://doi.org/10.1016/0034-4257\(93\)90096-G](https://doi.org/10.1016/0034-4257(93)90096-G)
- 829 Boschetti, M., Stroppiana, D., Brivio, P.A., Bocchi, S., 2009. Multi-year monitoring of rice crop
830 phenology through time series analysis of MODIS images. *Int J Remote Sens.* 30, 4643-4662.
831 <https://doi.org/10.1080/01431160802632249>
- 832 Borchers, A., Truex-Powell, E., Wallander, S., Nickerson, C., 2014. Multi-cropping practices: recent
833 trends in double-cropping (No. 1476-2017-3888).
- 834 Brown, M. E., De Beurs, K. M., & Marshall, M., 2012. Global phenological response to climate change in
835 crop areas using satellite remote sensing of vegetation, humidity and temperature over 26 years.
836 *Remote Sens. Environ.* 126, 174-183. <https://doi.org/10.1016/j.rse.2012.08.009>
- 837 Cong, N., Piao, S., Chen, A., Wang, X., Lin, X., Chen, S., Han, S., Zhou, G. Zhang, X., 2012. Spring
838 vegetation green-up date in China inferred from SPOT NDVI data: A multiple model analysis.
839 *Agric. For. Meteorol.* 165, 104-113. <https://doi.org/10.1016/j.agrformet.2012.06.009>
- 840 Congalton, R.G., 1991. A review of assessing the accuracy of classifications of remotely sensed data.
841 *Remote Sens. Environ.* 37, 35-46. [https://doi.org/10.1016/0034-4257\(91\)90048-B](https://doi.org/10.1016/0034-4257(91)90048-B)
- 842 Chen, C., Qian, C., Deng, A., Zhang, W., 2012. Progressive and active adaptations of cropping system to
843 climate change in Northeast China. *Eur J Agron.* 38, 94-103.
844 <https://doi.org/10.1016/j.eja.2011.07.003>
- 845 Chen, M., Griffis, T. J., Baker, J., Wood, J. D., Xiao, K., 2015. Simulating crop phenology in the
846 Community Land Model and its impact on energy and carbon fluxes. *J Geophys Res-Bioge.*
847 120(2), 310-325. <https://doi.org/10.1002/2014JG002780>
- 848 Chmielewski, F.-M., Müller, A., Bruns, E., 2004. Climate changes and trends in phenology of fruit trees
849 and field crops in Germany, 1961–2000. *Agr Forest Meteorol.* 121, 69-78.
850 [https://doi.org/10.1016/S0168-1923\(03\)00161-8](https://doi.org/10.1016/S0168-1923(03)00161-8)
- 851 Delbart, N., Kergoat, L., Toan, T.L., Lhermitte, J., Picard, G., 2005. Determination of phenological dates
852 in boreal regions using normalized difference water index. *Remote Sens. Environ.* 97, 26–38.
853 <https://doi.org/10.1016/j.rse.2005.03.011>
- 854 Diao, C. 2020. Remote sensing phenological monitoring framework to characterize corn and soybean
855 physiological growing stages. *Remote Sens. Environ.* 248, 111960.
856 <https://doi.org/10.1016/j.rse.2020.111960>
- 857 Fitzgerald, R. W., Lees, B. G., 1994. Assessing the classification accuracy of multisource remote sensing
858 data. *Remote Sens Environ.* 47(3), 362-368. [https://doi.org/10.1016/0034-4257\(94\)90103-1](https://doi.org/10.1016/0034-4257(94)90103-1)
- 859 Foody, G. M., Mathur, A., Sanchez-Hernandez, C., Boyd, D. S., 2006. Training set size requirements for
860 the classification of a specific class. *Remote Sens. Environ.* 104,1-14.
861 <https://doi.org/10.1016/j.rse.2006.03.004>
- 862 Gao, F., Anderson, M. C., Zhang, X., Yang, Z., Alfieri, J. G., Kustas, W. P., ... Prueger, J. H., 2017.
863 Toward mapping crop progress at field scales through fusion of Landsat and MODIS imagery.
864 *Remote Sens. Environ.* 9-25. <https://doi.org/10.1016/j.rse.2016.11.004>
- 865 Gilbert, R.O., 1987. *Statistical methods for environmental pollution monitoring.* John Wiley & Sons.

- 866 Gumma, M.K., Thenkabail, P.S., Maunahan, A., Islam, S., Nelson, A., 2014. Mapping seasonal rice
867 cropland extent and area in the high cropping intensity environment of Bangladesh using MODIS
868 500m data for the year 2010. ISPRS J Photogramm. 91, 98-113.
869 <https://doi.org/10.1016/j.isprsjprs.2014.02.007>
- 870 Guo, L., An, N., Wang, K., 2016. Reconciling the discrepancy in ground-and satellite-observed trends in
871 the spring phenology of winter wheat in China from 1993 to 2008. J Geophys Res: Atmos. 121,
872 1027–1042. <https://doi.org/10.1002/2015JD023969>
- 873 Hansen, N. C., Allen, B. L., Anapalli, S., Blackshaw, R. E., Lyon, D. J., Machado, S. 2016. Dryland
874 Agriculture in North America. In Innovations in Dryland Agriculture. Springer, Cham. 415-441.
875 https://doi.org/10.1007/978-3-319-47928-6_15
- 876 He, L., Asseng, S., Zhao, G., Wu, D. R., Yang, X. Y., Zhuang, W., et al. 2015. Impacts of recent climate
877 warming, cultivar changes, and crop management on winter wheat phenology across the Loess
878 Plateau of China. Agricultural and Forest Meteorology, 200, 135–143.
879 <https://doi.org/10.1016/j.agrformet.2014.09.011>
- 880 Heggenstaller, A. H., Anex, R. P., Liebman, M., Sundberg, D. N., Gibson, L. R., 2008. Productivity and
881 nutrient dynamics in bioenergy double-cropping systems. Agronomy Journal. 100(6), 1740-1748.
882 <https://doi.org/10.2134/agronj2008.0087>
- 883 Hmimina, G., Dufrêne, E., Pontailier, J. Y., Delpierre, N., Aubinet, M., Caquet, B., ... Gross, P., 2013.
884 Evaluation of the potential of MODIS satellite data to predict vegetation phenology in different
885 biomes: An investigation using ground-based NDVI measurements. Remote Sens. Environ., 132,
886 145-158. <https://doi.org/10.1016/j.rse.2013.01.010>
- 887 Hodges, T., 1991. Temperature and water stress effects on phenology. Predicting crop phenology, 7-13.
- 888 Hubert-Moy, L., Cotonnec, A., Le Du, L., Chardin, A., Pérez, P., 2001. A comparison of parametric
889 classification procedures of remotely sensed data applied on different landscape units. Remote
890 Sens. Environ. 75,174-187. [https://doi.org/10.1016/S0034-4257\(00\)00165-6](https://doi.org/10.1016/S0034-4257(00)00165-6)
- 891 Huang, X., Liu, J., Zhu, W., Atzberger, C., Liu, Q., 2019. The optimal threshold and vegetation index
892 time series for retrieving crop phenology based on a modified dynamic threshold method. Remote
893 Sens. 11(23), 2725. <https://doi.org/10.3390/rs11232725>
- 894 Huete, A., Didan, K., Miura, T., Rodriguez, E.P., Gao, X., Ferreira, L.G., 2002. Overview of the
895 radiometric and biophysical performance of the MODIS vegetation indices. Remote Sens
896 Environ. 83, 195-213. [https://doi.org/10.1016/S0034-4257\(02\)00096-2](https://doi.org/10.1016/S0034-4257(02)00096-2)
- 897 Huete, A. 1988. Huete, AR A soil-adjusted vegetation index (SAVI). Remote Sensing of Environment.
898 Remote Sens Environ. 25, 295-309. <http://hdl.handle.net/10453/13646>
- 899 Huete, A., Justice, C., Liu, H., 1994. Development of vegetation and soil indices for MODIS-EOS.
900 Remote Sens Environ. 49, 224-234. [https://doi.org/10.1016/0034-4257\(94\)90018-3](https://doi.org/10.1016/0034-4257(94)90018-3)
- 901 Huete, A., Justice, C., Van Leeuwen, W., 1999. MODIS vegetation index (MOD13). Algorithm
902 theoretical basis document, 3(213). https://modis.gsfc.nasa.gov/data/atbd/atbd_mod13.pdf
- 903 Huete, A.R., Liu, H.Q., Batchily, K., van Leeuwen, W., 1997. A comparison of vegetation indices over a
904 global set of TM images for EOS-MODIS. Remote Sens. Environ. 59 (3), 440–451.
905 [https://doi.org/10.1016/S0034-4257\(96\)00112-5](https://doi.org/10.1016/S0034-4257(96)00112-5)
- 906 Jiang, Z., Huete, A. R., Didan, K., & Miura, T. 2008. Development of a two-band enhanced vegetation
907 index without a blue band. Remote Sens Environ. 112(10), 3833-3845.
908 <https://doi.org/10.1016/j.rse.2008.06.006>
- 909 Jin, Z., Zhuang, Q., He, J.S., Luo, T. Shi, Y., 2013. Phenology shift from 1989 to 2008 on the Tibetan
910 Plateau: an analysis with a process-based soil physical model and remote sensing data. Clim
911 Change. 119(2), 435-449. <https://doi.org/10.1007/s10584-013-0722-7>
- 912 Kelley, K. W., Sweeney, D. W. 2005. Tillage and urea ammonium nitrate fertilizer rate and placement
913 affects winter wheat following grain sorghum and soybean. J Agron. 97(3), 690-697.
914 <https://doi.org/10.2134/agronj2004.0156>
- 915 Kisi, O., Ay, M. 2014. Comparison of Mann–Kendall
916 and innovative trend method for water quality parameters of the Kizilirmak River, Turkey. J
Hydrol. 513, 362-375. <https://doi.org/10.1016/j.jhydrol.2014.03.005>

- 917 Kisi, O., Ay, M., 2014. Comparison of Mann–Kendall and innovative trend method for water quality
918 parameters of the Kizilirmak River, Turkey. *J. Hydrol.* 513, 362-375.
919 <https://doi.org/10.1016/j.jhydrol.2014.03.005>
- 920 Kotsuki, S., Tanaka, K., 2015. SACRA – a method for the estimation of global high-resolution crop
921 calendars from a satellite-sensed NDVI. *Hydrol Earth Syst Sc.* 19, 4441-4461.
922 <https://doi.org/10.5194/hess-19-4441-2015>
- 923 Kucharik, C. J., 2006. A multidecadal trend of earlier corn planting in the central USA. *Agron J.* 98(6),
924 1544-1550. <https://doi:10.2134/agronj2006.0156>
- 925 Kukal, M. S., Irmak, S. 2018. US Agro-Climat in 20 th Century: Growing Degree Days, First and Last
926 Frost, Growing Season Length, and Impacts on Crop Yields. *Sci. Rep.* 8(1), 1-14.
927 <https://doi.org/10.1038/s41598-018-25212-2>
- 928 Li, L., Friedl, M., Xin, Q., Gray, J., Pan, Y., Frolking, S., 2014. Mapping crop cycles in China using
929 MODIS-EVI time series. *Remote Sens.* 6, 2473-2493. <https://doi.org/10.3390/rs6032473>
- 930 Liu, L., Wang, E., Zhu, Y., Tang, L., Cao, W., 2013. Quantifying three-decade changes of single rice
931 cultivars in China using crop modeling. *Field Crops Research*, 149, 84-94.
932 <https://doi.org/10.1016/j.fcr.2013.04.025>
- 933 Liu, L., Zhang, X., Yu, Y., Guo, W., 2017. Real-time and short-term predictions of spring phenology in
934 North America from VIIRS data. *Remote Sens Environ.* 194, 89-99.
935 <https://doi.org/10.1016/j.rse.2017.03.009>
- 936 Liu, Q., Li, X., Liu, G., Huang, C., Guo, Y., 2016a. Cotton area and yield estimation at Zhanhua county
937 of China using HJ-1 EVI time series. In, *ITM Web of Conferences* (p. 09001): EDP Sciences.
938 <https://doi.org/10.1051/itmconf/20160709001>
- 939 Liu, Q., Fu, Y., Zhu, Z., Liu, Y., Liu, Z., Huang, M., et al., 2016b. Delayed autumn phenology in the
940 Northern Hemisphere is related to change in both climate and spring phenology. *Global Change*
941 *Biol.* 22, 3702-3711. <https://doi.org/10.1111/gcb.13311>
- 942 Liu, Z., Wu, C., Liu, Y., Wang, X., Fang, B., Yuan, W., Ge, Q., 2017. Spring green-up date derived from
943 GIMMS3g and SPOT-VGT NDVI of winter wheat cropland in the North China Plain. *ISPRS J*
944 *Photogramm.* 130, 81-91. <https://doi.org/10.1016/j.isprsjprs.2017.05.015>
- 945 Lobell, D.B., Ortiz-Monasterio, J.I., Sibley, A.M., Sohu, V.S., 2013. Satellite detection of earlier wheat
946 sowing in India and implications for yield trends. *Agr Syst.* 115, 137-143.
947 <https://doi.org/10.1016/j.agsy.2012.09.003>
- 948 Lu, L., Wang, C., Guo, H., Li, Q., 2013. Detecting winter wheat phenology with SPOT-VEGETATION
949 data in the North China Plain. *Geocarto Int.* 29, 244-255.
950 <https://doi.org/10.1080/10106049.2012.760004>
- 951 Luo, Y., Zhang, Z., Chen, Y., Li, Z., Tao, F. 2020. ChinaCropPhen1km: a high-resolution crop
952 phenological dataset for three staple crops in China during 2000–2015 based on leaf area index
953 (LAI) products. *Earth Syst. Sci. Data.* 12(1). <https://doi.org/10.5194/essd-12-197-2020>
- 954 Marra, M. C., Carlson, G. A. 1986. Double-Cropping Wheat and Soybeans in the Southeast.
- 955 Martin, K. E. A., Hodgen, P. J., Freeman, K. W., Melchiori, R., Arnall, D. B., Teal, R. K., ... Stone, M. L.
956 2005. Plant-to-plant variability in corn production. *J Agron.* 97(6), 1603-1611.
957 <https://doi.org/10.2134/agronj2005.0129>
- 958 Menenti, M., Azzali, S., Verhoef, W., Van Swol, R., 1993. Mapping agro-ecological zones and time lag
959 in vegetation growth by means of Fourier analysis of time series of NDVI images. *Adv Space*
960 *Res.* 13 (5), 233–237. [https://doi.org/10.1016/0273-1177\(93\)90550-U](https://doi.org/10.1016/0273-1177(93)90550-U)
- 961 Mercier, A., Betbeder, J., Baudry, J., Le Roux, V., Spicher, F., Lacoux, J., ... Hubert-Moy, L., 2020.
962 Evaluation of Sentinel-1 & 2 time series for predicting wheat and rapeseed phenological stages.
963 *ISPRS J Photogramm.* 163, 231-256. <https://doi.org/10.1016/j.isprsjprs.2020.03.009>
- 964 Næsset, E. 1996. Conditional tau coefficient for assessment of producer's accuracy of classified remotely
965 sensed data. *ISPRS J Photogramm.* 51(2), 91-98. [https://doi.org/10.1016/0924-2716\(96\)00007-4](https://doi.org/10.1016/0924-2716(96)00007-4)

- 966 Nemani, R. R., Keeling, C. D., Hashimoto, H., Jolly, W. M., Piper, S. C., Tucker, C. J., ... Running, S.
 967 W., 2003. Climate-driven increases in global terrestrial net primary production from 1982 to
 968 1999. *Science*. 300(5625), 1560-1563. [10.1126/science.1082750](https://doi.org/10.1126/science.1082750)
- 969 Ogle, S.M.; Breidt, F.J.; Paustian, K. 2005. Agricultural management impacts on soil organic carbon
 970 storage under moist and dry climatic conditions of temperate and tropical regions.
 971 *Biogeochemistry*. 72, 87–121. <https://doi.org/10.1007/s10533-004-0360-2>
- 972 Ortiz-Monasterio, J.I., Lobell, D.B., 2007. Remote sensing assessment of regional yield losses due to sub-
 973 optimal planting dates and fallow period weed management. *Field Crop Res.* 101, 80-87.
 974 <https://doi.org/10.1016/j.fcr.2006.09.012>
- 975 Oteros, J., Garcia-Mozo, H., Botey, R., Mestre, A., Galan, C., 2015. Variations in cereal crop phenology
 976 in Spain over the last twenty-six years (1986-2012). *Clim Change*. 130, 545-558.
 977 <https://doi.org/10.1007/s10584-015-1363-9>
- 978 Pan, Z., Huang, J., Zhou, Q., Wang, L., Cheng, Y., Zhang, H., et al., 2015. Mapping crop phenology
 979 using NDVI time-series derived from HJ-1 A/B data. *Int J Appl Earth Obs.* 34, 188-197.
 980 <https://doi.org/10.1016/j.jag.2014.08.011>
- 981 Peltonen-Sainio, P., Jauhiainen, L., Hakala, K., Ojanen, H., 2009. Climate change and prolongation of
 982 growing season: changes in regional potential for field crop production in Finland. *Agr Food Sci.*
 983 <http://urn.fi/URN:NBN:fi-fe2015090311189>
- 984 Piao, S., Fang, J., Zhou, L., Ciais, P. Zhu, B., 2006. Variations in satellite-derived phenology in China's
 985 temperate vegetation. *Global Change Biol.* 12(4), 672-685. <https://doi.org/10.1038/nature06444>
- 986 Piao, S., Liu, Q., Chen, A., Janssens, I.A., Fu, Y., Dai, J., et al., 2019. Plant phenology and global climate
 987 change: current progresses and challenges. *Global Change Biol.* 25(6), 1922-1940.
 988 <https://doi.org/10.1111/gcb.14619>
- 989 Portmann, F. T., Siebert, S., Döll, P., 2010. MIRCA2000—Global monthly irrigated and rainfed crop
 990 areas around the year 2000: A new high-resolution data set for agricultural and hydrological
 991 modeling. *Global Biogeochem Cy*, 24(1). GB1011, [doi:10.1029/2008GB003435](https://doi.org/10.1029/2008GB003435)
- 992 Reed, B.C., 2013. Trend analysis of time-series phenology of North America derived from satellite data.
 993 *Gisci Remote Sens.* 43, 24-38. <https://doi.org/10.2747/1548-1603.43.1.24>
- 994 Ren, J., Chen, Z., Zhou, Q., Tang, H., 2008. Regional yield estimation for winter wheat with MODIS-
 995 NDVI data in Shandong, China. *Int J Appl Earth Obs.* 10, 403-413.
 996 <https://doi.org/10.1016/j.jag.2007.11.003>
- 997 Rezaei, E. E., Siebert, S., Ewert, F., 2017. Climate and management interaction cause diverse crop
 998 phenology trends. *Agr Forest Meteorol.* 233, 55-70.
 999 <https://doi.org/10.1016/j.agrformet.2016.11.003>
- 1000 Rezaei, E. E., Siebert, S., Hüging, H., Ewert, F., 2018. Climate change effect on wheat phenology
 1001 depends on cultivar change. *Sci. Rep.* 8(1), 1-10. <https://doi.org/10.1038/s41598-018-23101-2>
- 1002 Roerink, G., Menenti, M., Verhoef, W., 2000. Reconstructing cloudfree NDVI composites using Fourier
 1003 analysis of time series. *Int J Remote Sens.* 21, 1911-1917.
 1004 <https://doi.org/10.1080/014311600209814>
- 1005 Rouse, J.W., Hass, R.H., Schell, J.A. and Deering, D.W., 1974. Monitoring vegetation systems in the
 1006 Great Plains with ERTS., The 3rd earth resources technology satellite-1 symposium, Greenbelt,
 1007 MD, 309–317.
- 1008 Sacks, W.J., Deryng, D., Foley, J.A., Ramankutty, N., 2010. Crop planting dates: an analysis of global
 1009 patterns. *Global Ecol Biogeogr.* 19, 607-620. <https://doi.org/10.1111/j.1466-8238.2010.00551.x>
- 1010 Sacks, W.J., Kucharik, C.J., 2011. Crop management and phenology trends in the U.S. Corn Belt:
 1011 Impacts on yields, evapotranspiration and energy balance. *Agr Forest Meteorol.* 151, 882-894.
 1012 <https://doi.org/10.1016/j.agrformet.2011.02.010>
- 1013 Sakamoto, T., Yokozawa, M., Toritani, H., Shibayama, M., Ishitsuka, N., Ohno, H., 2005. A crop
 1014 phenology detection method using time-series MODIS data. *Remote Sens Environ.* 96, 366-374.
 1015 <https://doi.org/10.1016/j.rse.2005.03.008>

- 1016 Sakamoto, T., Van Nguyen, N., Ohno, H., Ishitsuka, N., Yokozawa, M., 2006. Spatio-temporal
1017 distribution of rice phenology and cropping systems in the Mekong Delta with special reference
1018 to the seasonal water flow of the Mekong and Bassac rivers. *Remote Sens Environ.* 100(1), 1-16.
1019 <https://doi.org/10.1016/j.rse.2005.09.007>
- 1020 Sakamoto, T. 2018. Refined shape model fitting methods for detecting various types of phenological
1021 information on major US crops. *ISPRS J Photogramm.* 138, 176-192.
1022 <https://doi.org/10.1016/j.isprsjprs.2018.02.011>
- 1023 Sakamoto, T., Wardlow, B.D., Gitelson, A.A., Verma, S.B., Suyker, A.E., Arkebauer, T.J., 2010. A Two-
1024 Step Filtering approach for detecting maize and soybean phenology with time-series MODIS
1025 data. *Remote Sens. Environ.* 114, 2146–2159. <https://doi.org/10.1016/j.rse.2010.04.019>
- 1026 Schwartz, M.D., Ahas, R., Aasa, A., 2006. Onset of spring starting earlier across the Northern
1027 Hemisphere. *Global Change Biol.* 12, 343-351. <https://doi.org/10.1111/j.1365-2486.2005.01097.x>
- 1028 Sen, P.K., 1968. Estimates of the regression coefficient based on Kendall's tau. *J Am Stat Assoc.* 63,
1029 1379-1389. <https://www.jstor.org/stable/2285891>
- 1030 Slayback, D. A., Pinzon, J. E., Los, S. O., Tucker, C. J., 2003. Northern hemisphere photosynthetic trends
1031 1982–99. *Global Change Biol.* 9(1), 1-15. <https://doi.org/10.1046/j.1365-2486.2003.00507.x>
- 1032 Son, N. T., Chen, C. F., Chen, C. R., Duc, H. N., Chang, L. Y., 2014. A phenology-based classification of
1033 time-series MODIS data for rice crop monitoring in Mekong Delta, Vietnam. *Remote Sens.* 6(1),
1034 135-156. <https://doi.org/10.3390/rs6010135>
- 1035 Sparks, T., Croxton, P., Collinson, N., Taylor, P.W., 2005. Examples of phenological change, past and
1036 present, in UK farming. *Ann Appl Biol.* 146, 531-537. <https://doi.org/10.1111/j.1744-7348.2005.050016.x>
- 1037
- 1038 Tao, F., Yokozawa, M., Xu, Y., Hayashi, Y., Zhang, Z., 2006. Climate changes and trends in phenology
1039 and yields of field crops in China, 1981–2000. *Agr Forest Meteorol.* 138, 82-92.
1040 <https://doi.org/10.1016/j.agrformet.2006.03.014>
- 1041 Tao, F., Zhang, S., Zhang, Z., 2012. Spatiotemporal changes of wheat phenology in China under the
1042 effects of temperature, day length and cultivar thermal characteristics. *Eur J Agron.* 43, 201-212.
1043 <https://doi.org/10.1016/j.eja.2012.07.005>
- 1044 Tao, F., Zhang, S., Zhang, Z., and Rotter, R. P. 2014. Maize growing duration was prolonged across
1045 China in the past three decades under the combined effects of temperature, agronomic anagement,
1046 and cultivar shift, *Glob Change Biol.* 20, 3686–3699. <https://doi.org/10.1111/gcb.12684>
- 1047 Taylor, R.D., Won, W. K., 2015. Outlook of the US and World Corn and Soybean Industries. 2015-2024.
- 1048 Thompson, J.A., Paull, D.J., 2017. Assessing spatial and temporal patterns in land surface phenology for
1049 the Australian Alps (2000–2014). *Remote Sens Environ.* 199, 1-13.
1050 <https://doi.org/10.1016/j.rse.2017.06.032>
- 1051 Thornton, M., Thornton, P., Wei, Y., Vose, R., Boyer, A., 2017. Daymet: Daily Surface Weather Data on
1052 a 1-km Grid for North America, Version 3. ORNL DAAC, Oak Ridge, Tennessee, USA.
- 1053 Tveito, O.E., Bjørndal, I., Skjelvåg, A.O. Aune, B., 2005. A GIS-based agro-ecological decision system
1054 based on gridded climatology. *Meteorol Appl.* 12(1), 57-68.
1055 <https://doi.org/10.1017/S1350482705001490>
- 1056 Wang, J., Wang, E. L., Feng, L. P., Yin, H., Yu, W. D. 2013. Phenological trends of winter wheat in
1057 response to varietal and temperature changes in the North China Plain. *Field Crops Res.* 144,
1058 135–144. <https://doi.org/10.1016/j.fcr.2012.12.020>
- 1059 Wang, S., Mo, X., Liu, Z., Baig, M.H.A., Chi, W., 2017. Understanding long-term (1982–2013) patterns
1060 and trends in winter wheat spring green-up date over the North China Plain. *Int J Appl Earth Obs.*
1061 57, 235-244. <https://doi.org/10.1016/j.jag.2017.01.008>
- 1062 Wang, Z., Chen, J., Li, Y., Li, C., Zhang, L., Chen, F., 2016. Effects of climate change and cultivar on
1063 summer maize phenology. *Int J Plant Prod.* 10, 509-525. <https://doi.org/10.22069/IJPP.2016.3046>
- 1064 Wang, Z. B., Chen, J., Tong, W. J., Xu, C. C., Chen, F. 2018. Impacts of climate change and varietal
1065 replacement on winter wheat phenology in the north China Plain. *Int. J. Plant Prod.*
1066 <https://doi.org/10.1007/s42106-018-0024-0>

- 1067 White, K., Pontius, J., Schaberg, P., 2014. Remote sensing of spring phenology in northeastern forests: A
1068 comparison of methods, field metrics and sources of uncertainty. *Remote Sens Environ.* 148, 97-
1069 107. <https://doi.org/10.1016/j.rse.2014.03.017>
- 1070 White, M.A., de Beurs, K.M., Didan, K., Inouye, D.W., Richardson, A.D., Jensen, O.P., et al., 2009.
1071 Intercomparison, interpretation, and assessment of spring phenology in North America estimated
1072 from remote sensing for 1982-2006. *Global Change Biol.* 15, 2335-2359.
1073 <https://doi.org/10.1111/j.1365-2486.2009.01910.x>
- 1074 White, M.A., Thornton, P.E., Running, S.W., 1997. A continental phenology model for monitoring
1075 vegetation responses to interannual climatic variability. *Glob. Biogeochem. Cycles* 11, 217–234.
1076 <https://doi.org/10.1029/97GB00330>
- 1077 Wu, W. B., Peng, Y., Tang, H. J., Zhou, Q. B., Chen, Z. X., Shibasaki, R., 2010. Characterizing spatial
1078 patterns of phenology in cropland of China based on remotely sensed data. *Agr Sci China*, 9(1),
1079 101-112. [https://doi.org/10.1016/S1671-2927\(09\)60073-0](https://doi.org/10.1016/S1671-2927(09)60073-0)
- 1080 Xin, J., Yu, Z., Louise, V.L., Paul, M.D., 2002. Mapping crop key phenological stages in the North China
1081 Plain using NOAA time series images. *Int J Appl Earth Obs.* 4, 109-117.
1082 [https://doi.org/10.1016/S0303-2434\(02\)00007-7](https://doi.org/10.1016/S0303-2434(02)00007-7)
- 1083 Xu, X., Conrad, C., Doktor, D., 2017. Optimising phenological metrics extraction for different crop types
1084 in Germany using the moderate resolution imaging spectrometer (MODIS). *Remote Sens.* 9, 254.
1085 <https://doi.org/10.3390/rs9030254>
- 1086 Yan, H., Liu, F., Qin, Y., Niu, Z., Doughty, R., Xiao, X., 2019. Tracking the spatio-temporal change of
1087 cropping intensity in China during 2000-2015. *Environ Res Lett.* 14(3).
1088 <https://doi.org/10.1088/1748-9326/aaf9c7>
- 1089 Yan, H., Xiao, X., Huang, H., Liu, J., Chen, J., Bai, X., 2014. Multiple cropping intensity in China
1090 derived from agro-meteorological observations and MODIS data. *Chinese Geogr Sci.* 24, 205-
1091 219. <https://doi.org/10.1007/s11769-013-0637-2>
- 1092 You, L., Wood, S., Wood-Sichra, U., Wu, W., 2014. Generating global crop distribution maps: From
1093 census to grid. *Agric. Syst.* 127, 53-60. <https://doi.org/10.1016/j.agsy.2014.01.002>
- 1094 You, X., Meng, J., Zhang, M., Dong, T., 2013. Remote sensing based detection of crop phenology for
1095 agricultural zones in China using a new threshold method. *Remote Sens.* 5(7), 3190-3211.
1096 <https://doi.org/10.3390/rs5073190>
- 1097 Yu, Y. Q., Huang, Y., and Zhang, W., 2012. Changes in rice yields in China since 1980 associated with
1098 cultivar improvement, climate and crop management, *Field Crop. Res.*, 136, 65–75,
1099 <https://doi.org/10.1016/j.fcr.2012.07.021>
- 1100 Zeng, L., Wardlow, B., Wang, R., Shan, J., Tadesse, T., Hayes, M., Li, D., 2016. A hybrid approach for
1101 detecting corn and soybean phenology with time-series MODIS data. *Remote Sens Environ.* 181,
1102 237-250. <https://doi.org/10.1016/j.rse.2016.03.039>
- 1103 Zeng, L., Wardlow, B. D., Xiang, D., Hu, S., Li, D., 2020. A review of vegetation phenological metrics
1104 extraction using time-series, multispectral satellite data. *Remote Sens Environ.* 237, 111511.
1105 <https://doi.org/10.1016/j.rse.2019.111511>
- 1106 Zhang, G., Xiao, X., Dong, J., Kou, W., Jin, C., Qin, Y., et al., 2015. Mapping paddy rice planting areas
1107 through time series analysis of MODIS land surface temperature and vegetation index data.
1108 *ISPRS J Photogramm.* 106, 157-171. <https://doi.org/10.1016/j.isprsjprs.2015.05.011>
- 1109 Zhang, S., Tao, F. L., and Zhang, Z. 2014. Rice reproductive growth duration increased despite of
1110 negative impacts of climate warming across China during 1981–2009, *Eur. J. Agron.* 54, 70–83.
1111 <https://doi.org/10.1016/j.eja.2013.12.001>
- 1112 Zhang, X., Friedl, M.A., Schaaf, C.B., Strahler, A.H., Hodges, J.C.F., Gao, F., Reed, B.C., Huete, A.,
1113 2003. Monitoring vegetation phenology using MODIS. *Remote Sens. Environ.* 84, 471–475.
1114 [https://doi.org/10.1016/S0034-4257\(02\)00135-9](https://doi.org/10.1016/S0034-4257(02)00135-9)
- 1115 Zhang, X., Liu, L., Henebry, G., 2019. Impacts of land cover and land use change on long-term trend of
1116 land surface phenology: a case study in agricultural ecosystems. *Environ Res Lett.* 14, 12.
1117 <https://doi.org/10.1088/1748-9326/ab04d2>

- 1118 Zhang, X., Wang, J., Henebry, G. M., Gao, F. 2020. Development and evaluation of a new algorithm for
1119 detecting 30 m land surface phenology from VIIRS and HLS time series ISPRS J Photogramm.
1120 161, 37-51. <https://doi.org/10.1016/j.isprsjprs.2020.01.012>
- 1121 Zheng, H., Cheng, T., Yao, X., Deng, X., Tian, Y., Cao, W., Zhu, Y., 2016. Detection of rice phenology
1122 through time series analysis of ground-based spectral index data. Field Crop Res. 198, 131-139.
1123 <https://doi.org/10.1016/j.fcr.2016.08.027>
- 1124 Zheng, Y., Wu, B., Zhang, M., Zeng, H., 2016. Crop phenology detection using high spatio-temporal
1125 resolution data fused from SPOT5 and MODIS products. Sensors. 16.
1126 <https://doi.org/10.3390/s16122099>
- 1127 Zhou, J., Jia, L., Menenti, M., 2015. Reconstruction of global MODIS NDVI time series: Performance of
1128 Harmonic ANalysis of Time Series (HANTS). Remote Sens Environ, 163, 217-228.
1129 <https://doi.org/10.1016/j.rse.2015.03.018>
- 1130 Zhu, W., Tian, H., Xu, X., Pan, Y., Chen, G., Lin, W., 2012. Extension of the growing season due to
1131 delayed autumn over mid and high latitudes in North America during 1982–2006. Global Ecol
1132 Biogeogr. 21, 260-271. <https://doi.org/10.1111/j.1466-8238.2011.00675>
- 1133